On the retrieval of columnar aerosol mass and CCN concentration by MODIS

Santiago Gassó
Goddard Earth Science and Technology Center, University of Maryland, Baltimore County, Baltimore, Maryland, USA

Dean A. Hegg
Department of Atmospheric Science, University of Washington, USA

Received 27 March 2002; revised 23 May 2002; accepted 24 May 2002; published 8 January 2003.

[1] A parameterization is introduced for the derivation of columnar aerosol mass concentration (AMC) and cloud condensation nucleus concentration (CCNC) from the primary aerosol products of Moderate-Resolution Imaging Spectroradiometer (MODIS). The method relies on the scaling between AMC and optical depth with a proportionality constant dependent on MODIS-derived r_{eff}, η (contribution of the accumulation mode radiance to the total radiance), ambient RH, and an assumed constant aerosol composition. The CCNC is derived from a parameterization of concentration as a function of the retrieved aerosol volume. By comparing with in situ data, it is shown that retrievals in dry ambient conditions (dust) are improved when using a proportionality constant dependent on r_{eff} and η obtained in the same pixel. In high-humidity environments, the improvement in the new method is inconclusive because of the difficulty in accounting for the uneven vertical distribution of relative humidity. Additionally, two detailed comparisons of AMC and CCNC retrieved by the MODIS Airborne Simulator (MAS) algorithm and the new method are shown. The new method and MAS retrievals of AMC are within the same order of magnitude with respect to the in situ measurements of aerosol mass. However, the proposed method is closer to the in situ measurements than the MODIS retrievals. The retrievals of CCNC are also within the same order of magnitude for both methods. Finally, the new method is applied to an actual MODIS retrieval. Although no in situ data is available for comparison, it is shown that the proposed method yields more credible values than the MODIS retrievals. *INDEX TERMS:* 1640 Global Change: Remote sensing; 3360 Meteorology and Atmospheric Dynamics: Remote sensing; *KEYWORDS:* CCN, aerosol mass, validation, MODIS

Citation: Gassó, S., and D. A. Hegg, On the retrieval of columnar aerosol mass and CCN concentration by MODIS, *J. Geophys. Res.*, *108*(D1), 4010, doi:10.1029/2002JD002382, 2003.

1. Introduction

[2] The energy balance of the ocean atmosphere-system can be modified by the presence of aerosols in the atmosphere [*Ramanathan et al.*, 2001a]. They can act indirectly through the modification of clouds optical properties, rain patterns and lifetime [*Albrecht*, 1989; *Rosenfeld et al.*, 2001]. More directly, aerosols reflect solar radiation and, depending on composition, can be strong absorbers of solar radiation resulting in perturbations in regional climate [*Penner et al.*, 1992, 1998; *Haywood and Ramaswamy*, 1998; *Haywood et al.*, 1997]. As a consequence, aerosol research is an important component in climate studies. In broad terms, aerosols are being studied in with three different methodologies. The first approach is the modeling of global distribution and chemical processes in which aerosols take part. These computations are essential for the prediction of the aerosol effects in Global Climate Models (GCMs). A key issue in the validity of such complex model computations is the reliability of the parameterizations used and how accurately variables are predicted. It is at this point where the other two methodologies come into play. These methodologies, satellite and in situ measurements, provide invaluable tools to compare model predictions with the actual parameters. In situ measurements provide the information by measuring directly the properties of interest. They are obtained by means of permanent ground stations for example, the NOAA-CMDL network [*Ogren*, 1995] or by intensive field campaigns such as INDOEX [*Ramanathan et al.*, 2001b] or ACE-2 [*Raes et al.*, 2000]. With respect to satellite retrievals, global measurements of aerosol optical depth obtained from space were limited to values derived by relatively extensive AVHRR database [*Durkee et al.*, 1991; *Husar et al.*, 1997]. However, the AVHRR detector was not designed for aerosol retrievals and the

0148-0227/03/2002JD002382$09.00

two channels used for retrievals had calibration drift problems as well as the difficulty of applying a water vapor correction. These problems significantly impact the accuracy of optical depth retrievals [*Mishchenko et al.*, 1999]. In addition, aerosol optical depth is not necessarily the prognostic variable of aerosol chemical models, which in fact usually predict parameters such as aerosol columnar mass and number concentrations. Nevertheless, several attempts have been made to compare AVHRR retrievals of optical depths with the same parameters derived from global aerosol models [*Chin et al.*, 2002; *Penner et al.*, 2002]. Ground based network of radiometers such as AERONET [*Holben et al.*, 2001] in many ways complements the space-borne retrievals by improving the temporal coverage in one region. However, such networks lack the global coverage needed for comparisons with global models. Recently deployed space-borne platforms carry detectors with improved calibration procedures, ground coverage and channels suitable for retrieval of a number of aerosol columnar properties in addition to optical depth. For example, with Moderate-Resolution Imaging Spectroradiometer (MODIS; onboard the Terra satellite launched in December 1999), the capabilities for deriving aerosol properties from space have been expanded. In particular, the MODIS aerosol algorithm is able to derive the aerosol optical depth at several wavelengths, columnar aerosol effective radius (r_{eff}), and the contribution of the accumulation mode to the total radiance in the column ($\eta = I_{acc}/I_{total}$) [*Tanré et al.*, 1997]. The availability of τ, r_{eff} and η in each pixel and the fact that the retrieval is expected to be more accurate [*King et al.*, 1992] should appreciably improve the utility of the data. As secondary products, the MODIS aerosol algorithm derives other columnar properties such as CCN concentrations and aerosol volume [*Tanré et al.*, 1999]. Additionally, MODIS is capable of deriving an estimation of the mean relative humidity in the low troposphere from the infrared channels [*Menzel and Gumley*, 1998]. The breadth of new data is expected to be very useful for global real time monitoring as well as comparison with GCM. However, the retrieval of aerosol properties from space (passive remote sensing) is inherently indirect and the amount of information available from the spectral dependence of the measured radiance is limited. For example, in the case of the MODIS aerosol algorithm, the accuracy of some of the secondary products derived, specifically total columnar aerosol mass (or burden) and number concentration is uncertain.

[3] The objective of this paper is to offer an alternative method, and possibly more accurate, for the retrieval of aerosol burden and concentration by using the scaling between optical depth and aerosol mass. The method makes use of the primary products derived by the MODIS aerosol algorithm to customize the proportionality between the two parameters in each pixel (section 2). In order to demonstrate the applicability of the method, we utilize data from the ACE-2 [*Russell and Heintzenberg*, 2000] and TARFOX [*Russell et al.*, 1999] campaigns (section 3). During both experiments, collocated measurements of sunphotometer optical depth onboard an aircraft and in situ aerosol data profiles were gathered in polluted and dust laden atmospheres. A parameterization of the proportionality constant between mass and optical depth is obtained and applied to satellite and sunphotometer retrieval of properties of different aerosol types encountered in TARFOX and ACE-2. Then, the retrieved mass is used for derivation of aerosol concentration and compare with measured values (section 4). Finally, an application of the method is shown in actual MODIS pictures (section 5).

2. Methodology

2.1. Proposed Method

[4] Spaceborne retrievals of aerosol mass were first reported by *Griggs* [1975] and *Fraser* [1976]. The latter used Landsat pictures (3 visible bands and one in the near infrared) and the method was based on comparison of modeled and measured radiances. Aerosol properties were extracted from the aerosol model parameters that best matched the measured radiance. Other authors have attempted different retrieval techniques with different satellite detector like AVHRR [*Ferrare et al.*, 1990; *Liousse et al.*, 1997] or METEOSAT [*Dulac et al.*, 1992] but all of these methods have in common a mathematical formula that relates the aerosol burden to an optical parameter such as radiance [*Griggs*, 1975; *Fraser*, 1976] or optical depth [*Fraser et al.*, 1984; *Kaufman and Fraser*, 1990]. Because the methods have been applied to aerosol events such as large-scale dust or smoke plumes, it has been possible to utilize an a priori knowledge of the aerosol under observation to determine the proportionality constant between mass and radiance (or optical depth). All the above studies provide only minimal satisfactory evidence to verify these methods.

[5] The approach utilized in this study is similarly based on *Fraser et al.* [1984], a methodology for routine retrievals of aerosol mass from the GOES platform (one visible channel). In this case, the method (referred to as the ''Fraser method'' throughout this study) consists of first retrieving an optical depth and then apply a scaling between mass and total extinction over the column. This relationship is defined from the integration of the optical properties throughout the column:

$$m_{col} = \int_0^{z_{TOA}} M_{aer}(z)dz = \int_0^{z_{TOA}} \frac{\sigma_{sp}(z,\lambda)}{\alpha_{sp}(z,\lambda)}dz \qquad (1)$$

where $\sigma_{sp}(z, \lambda)$ is the particle scattering coefficient, $M_{aer}(z)$ is the aerosol mass per unit of volume of air, m_{col} is the total aerosol mass in the column (units mass/area) and $\alpha_{sp}(z, \lambda)$ is the mass scattering efficiency (mse). The mse is an intensive parameter defined as the ratio of the scattering coefficient to the amount of mass contained in a unit volume of air (m^2/g) at wavelength λ:

$$\alpha_{sp}(\lambda) = \frac{\sigma_{sp}(\lambda)}{M_{aer}} = \frac{\pi \int n(r)r^2 Q_{sca}(r,\lambda,m)dr}{\frac{4\pi}{3}\int \rho(r)n(r)r^3 dr} \qquad (2)$$

where r = particle radius, n(r) = number of particles with radius r, $\rho(r)$ = density of the particle, m(r) = index of refraction of particle r and $Q_{sca}(r, \lambda, m)$ = scattering efficiency. Equation (2) can be extended to define the mass extinction efficiency, which relates aerosol mass with the aerosol extinction coefficient, by replacing Q_{sca} with

Q_{ext}. The magnitude of mse is dependent on the aerosol composition and on the location of the size distribution with respect to the active optical range (Mie peaks). For example, aerosol size distributions with a large concentration of particles in the accumulation mode have an mse ranging from 2 to 6.5 m^2/g (measured at dry conditions) depending on the composition [*Quinn et al.*, 1998; *Reid et al.*, 1998; *Richards et al.*, 1999]. Because Q_{sca}, (or Q_{ex}) is approximately proportional to r in this size range, the mse is exclusively dependent on composition through the changes in Q_{sca} (or Q_{ext}) since the numerator and denominator in equation (2) approximately scale with each other. However, in distributions with large contributions of particles in the coarse mode, such as those found in clean marine environments or dust, the efficiency Q tends to be constant ($\sim$2) regardless of the size of the particle and this results in a mse ranging 0.2–1.2 m^2/g [*Li-Jones et al.*, 1998; *Malm and Day*, 2000; *Maring et al.*, 2000; *Andreae et al.*, 2002]. The assumption in the Fraser method is that α_{sp} and parameters such as ambient humidity and single scattering albedo are constant in the atmospheric column. This assumption, although necessary because of the limited information available in a passive detector, is not always correct [*Collins et al.*, 2000; *Schmeling et al.*, 2000]. Also, within an aerosol layer with homogenous composition, the mse may be variable because of the contribution of particles from different modes to the total scattering, or variations in local humidity. For example, this is the case in a marine boundary layer with a large concentration of coarse mode particles near the sea surface and with conditions of low mixing, which tends to concentrate large particles at the bottom of the column.

[6] With an assumption of constant properties in the column, equation (1) can be related to the measured optical depth (τ_{ex}) by:

$$m_{col} = \frac{\omega_0 \tau_{ex}}{\alpha_{sp}} \tag{3}$$

where the single scattering albedo (ω_o) is defined as the ratio of σ_{sc}/σ_{ext}. As with all the studies referenced earlier, it has been possible to utilize an a priori knowledge of the aerosol under observation to determine the proportionality constant between mass and radiance (or optical depth), the constant being the ratio of single scattering albedo to mse.

[7] The relationship between columnar mass and optical depth was further expanded by *Kaufman and Fraser* [1990] who utilized an interesting approach with AVHRR data. The retrieval algorithm derived simultaneously the optical depth (τ), single scattering albedo (ω_o) and the geometric mass radius of the size distribution (r_m, assumed as a monolog-normal) by means of a look-up table. Once these parameters are determined, the columnar mass concentration is derived by using:

$$m_{col} = c(r_m) \cdot \tau_{ext} \tag{4}$$

where $c(r_m)$ is the columnar mass concentration-extinction ratio (units = mass/area). Because *Kaufman and Fraser* [1990] were studying smoke, the aerosol composition could be assumed. Then, the ratio is parameterized as a function of r_m for several smoke aerosol models. In this way, the method derives the aerosol columnar mass in each pixel by customizing the proportionality constant and by using all information available in a self-consistent manner.

[8] A key point to note in assessing these retrievals is that the aerosol mass retrieved by equation (4) corresponds to a retrieval in ambient conditions. This is an important point for two reasons. From the standpoint of validation of retrievals, airborne and ground in situ measurements are commonly made at a reference relative humidity RH_o (usually below 40%). Thus, prior to comparing in situ measurements with satellite retrievals, a RH correction must be applied to the remotely sensed data. In the case of *Fraser et al.* [1984], this correction was assumed constant for the whole scene. Associated with this, when using satellite retrievals of aerosol mass, it is critical to determine the contribution of water in the aerosol. This is important for studies of the effect of aerosols on clouds since it is the aerosol dry mass that modulates the indirect effect [*Boucher and Lohmann*, 1995] and for comparison of global distributions of aerosol with the outputs of global geochemical models which output total dry mass [*Langner and Rodhe*, 1991].

[9] Summarizing, in the Fraser method, all parameters but the optical depth are assumed. The improvement proposed here is to derive some of these parameters from additional information available from the same platform.

[10] We propose a parameterization of the proportionality constant in equation (4) as a function of the primary aerosols parameters derived by the MODIS aerosol algorithm. Specifically, we will use a parameterization of the mse as a function of r_{eff} and η and parameterization of the hygroscopic factor as a function of ambient RH and assumed hygroscopic exponent. In contrast to the *Fraser et al.* [1984] study, we will use an estimation of the mean ambient RH derived from remote sensing rather than simply assume an RH based on the venue.

2.2. Assumptions and Uncertainties

[11] The simplicity of equation (3) is based on several important assumptions: i) intensive aerosol size distribution parameters and dry composition are constant with altitude ii) ambient RH is constant with altitude iii) single scattering albedo is constant throughout the column. Clearly, most of these conditions are not always present. However, they are frequently found in a climatological sense (i.e., when considering the distributions of humidity and aerosols in monthly or yearly averages). Similarly, while there are no studies indicating the frequency of coincidence of high humidity with aerosol layers, some of the assumptions listed above have been addressed. With respect to aerosol dry properties, *Sheridan and Ogren* [1999] showed that aerosol intensive properties such as dry ω_o or dry backscattering ratio are fairly homogeneously distributed in the BL and ground measurements of those parameters are representative of columnar values in the low troposphere in a climatological sense. Also, they showed that most of the aerosol extinction occurs at low altitudes, generally in the BL. The study was carried out using data from several airborne campaigns in the south and northeast of the US. A well-mixed boundary layer (including RH and aerosols) is a scenario frequently found in marine environments in a

climatological sense, i.e., timescales of months or weeks. However, daily variability can be significant when comparing with weekly or monthly averages [*Hsu and Blanchard*, 1989].

[12] As was mentioned at the end of section 2.1, the retrieval of columnar aerosol mass (or volume, since the density is assumed) involves a correction for hygroscopicity. This implies that a correction should be applied either to the ambient optical depth so it can be compared with the dry in situ data, or to correct the measured dry sized distributions to ambient conditions. The latter approach was utilized by several authors in different field campaigns [*Clarke et al.*, 1996, 2001; *Hartley et al.*, 2000; *Collins et al.*, 2000; *Redemann et al.*, 2000]. Such column closure studies have shown mixed results, because of a combination of problems including inefficiencies in the instrumentation, unknown aerosol composition and inlet sampling probe. The cited studies had to rely on a number of assumptions in order to adjust the dry in situ data to match ambient conditions.

[13] Another approach is the correction to dry conditions of the optical depth. Since the behavior of aerosol scattering with humidity is known, the correction to dry conditions of the optical depth is of the form:

$$\tau_{sc}(RH_{amb}) = \tau_{sc}(RH_o) \cdot \left(\frac{1 - RH_{amb}}{1 - RH_o}\right)^{-\gamma} \quad (5)$$

where RH_o is a reference relative humidity (usually 30–40%). Equation (5) is the natural extension of the Kasten equation [*Kasten*, 1969; *Hänel*, 1976], which is based on observations of aerosol scattering as a function of relative humidity. The exponent γ depends on the hygroscopic nature of the aerosol and it has been shown to vary in ambient aerosols according to their chemical composition [*Hänel*, 1976; *Hegg et al.*, 1996; *Carrico et al.*, 2000]. Note that equation (5) assumes that RH_{amb} and γ are constant in the column and that RH(z) scales with $\sigma_{sp}(z)$. This is a very common approximation utilized in remote sensing applications [*Kaufman and Fraser*, 1983; *Hitzenberger and Rizzi*, 1993; *Remer et al.*, 1997]. However, it is not supported by in situ measurements of aerosol hygroscopicity in the column [*Kotchenruther et al.*, 1999; *Gassó et al.*, 2000]. A similar approach is applied to the single scattering albedo, that is, it is assumed that $\omega_o = \tau_{sc}/\tau_{ex} = \sigma_{sc}/\sigma_{ex}$.

[14] Then, the expression for retrieving the total dry aerosol mass in the column ($m_{col}(RH_o)$) results from the combination of equation (5) with equation (3):

$$m_{col}(RH_o) = \frac{\tau_{ext}(RH_{amb}, \lambda). \cdot \omega_o(RH_{amb}, \lambda)}{\alpha_s(RH_o, \lambda) \cdot F(RH_{amb}, RH_o, \gamma)} \quad (6)$$

where $F(RH_{amb}, RH_o, \gamma)$ is the second factor on the rhs of equation (5). The uncertainty of equation (6) is:

$$\frac{\Delta m_{col}}{m_{col}} = \pm\left[\left(\frac{\Delta\alpha_s}{\alpha_s}\right)^2 + \left(\frac{\Delta\omega_o}{\omega_o}\right)^2 + \left(\frac{\Delta F}{F}\right)^2 + \left(\frac{\Delta\tau_{ext}}{\tau_{ext}}\right)^2\right]^{1/2} \quad (7)$$

The uncertainty in humidity correction F is computed as:

$$\Delta F(RH, RH_o, \gamma) = \left[\left(\frac{\partial F}{\partial RH}\Delta RH\right)^2 + \left(\frac{\partial F}{\partial RH_o}\Delta RH_o\right)^2 + \left(\frac{\partial F}{\partial \gamma}\Delta\gamma\right)^2\right]^{1/2} \quad (8)$$

where RH is the ambient RH, RH_o is the reference RH (i.e., the RH at which the in situ aerosol was sampled) and γ is the aerosol hygroscopic exponent. Equations (6) and (7) are used to obtain a measurement of aerosol mass (and uncertainty) in the column.

2.3. Experimental Data

[15] The experimental data utilized in this paper are extracted from databases generated during two field experiments. One of them is the Troposphere Aerosol Radiative Forcing Experiment (TARFOX)that took place during the summer of 1996 on the US Mid Atlantic seaboard [*Russell et al.*, 1999] to study aerosols advected off the East Coast. The plume extending from the U.S. east coast provides an excellent opportunity to isolate and study aerosols generated by human industrial activity, and to measure the magnitude and uncertainty of the direct radiative forcing due to these aerosols. In situ measurements were made by aircraft and remote sensing measurements were made by ground-based, airborne, and four satellite platforms. This resulted in the collection of a unique aerosol data set in a very heavily polluted airshed. In particular, the data utilized in this study was gathered by the University of Washington C131 aircraft, which carried a sunphotometer on aboard as well as a complete suite of aerosol instrumentation. Previous studies of the TARFOX data set [*Hartley et al.*, 2000; *Redemann et al.*, 2000] have shown that the vertical structure of the aerosol was stratified in two or three layers very frequently. Additionally, air masses with significant levels of humidity in the FT, occasionally containing high aerosol concentrations, were observed.

[16] The second data set corresponds to the data obtained during the Aerosol Characterization Experiment 2 (ACE-2). The experiment took place during June and July 1997 in the Portugal–Canary Island corridor with the specific purpose of studying physical and chemical properties of the typical aerosols found in that area. Of the six aircrafts involved in the experiment, only the CIRPAS Pelican aircraft carried instrumentation suitable for the simultaneous comparisons of retrieved and measured aerosol columnar mass [*Russell and Heintzenberg*, 2000]. Specifically the Pelican carried onboard a 14 wavelength sunphotometer [*Schmid et al.*, 2000] along with four size distribution measuring devices [*Collins et al.*, 2000]. Additionally, instrumentation for measuring aerosol optical [*Öström and Noone*, 2000] and hygroscopic [*Gassó et al.*, 2000] properties as well as some composition measurements were available [*Schmeling et al.*, 2000]. Of the 23 flights, only 6 were dedicated to studies of clear sky columnar aerosol optical properties. In these cases, the Pelican encountered different aerosol masses. They were identified according to their origin and composition: marine aerosol influenced by continental anthropogenic sources, marine aerosols originated from unpolluted areas in the North Atlantic, dust and free tropospheric aerosols. The first two were always encountered in the marine boundary layer whereas the latter two were always detected above the BL. As will be explained later, only data from the profiles in dust were utilized in this study.

2.4. Processing of Data

[17] The data used from TARFOX were obtained aboard the University of Washington's (UW) C-131A research. A

comprehensive description of the C131 instruments is given by *Hobbs* [1999]. The data relevant for the analysis presented here follows the same data adjustments and procedures of *Hartley et al.* [2000] and *Hartley* [2000]. In this section we briefly describe the instruments of particular importance to this study and we emphasize the adjustments that differed to those applied by *Hartley et al.* [2000].

[18] The NASA-Ames six-channel, Auto-Tracking Sunphotometer (AATS-6) was mounted on top of the fuselage of the UW C131-A. The instrument operates by tracking the Sun and measuring the intensity of the solar beam at central wavelengths of 380, 451, 526, 861, 940, and 1021 nm, with narrow channel full widths at half maximum (FWHM) of 5 nm [*Matsumoto*, 1987]. Comparison of the intensity at any height with the known intensity at the top of the atmosphere determines the total optical depth (i.e., due to the combined effects of gases, aerosols, and clouds) of the atmospheric layer between the aircraft and the top of the atmosphere. *Russell et al.* [1993] discusses the mechanics of deducing aerosol optical depth from measurements of total optical depth. During TARFOX there were mechanical problems with the 861 nm channel. Hence, the data from that channel was unusable for analysis. The 940 nm channel is centered on a water vapor absorption band and was used to infer column water vapor, rather than aerosol properties. The four remaining channels (380, 451, 526, and 1021 nm) were used for deducing aerosol optical depth in TARFOX.

[19] The MODIS Airborne Simulator (MAS) is an airborne version of MODIS carried on-board a NASA ER-2 high-altitude research aircraft. The instrument is described by *King et al.* [1996]. It is a scanning spectrometer with 50 channels but only the 5 channels centered at λ = 549, 655, 867, 1643 and 2105 nm, equivalent to the MODIS/Terra channels, were used during TARFOX. The instrument is flown at an altitude of 20 km and it scans in the across-track direction. The swath width is 36 km. The spatial resolution is 50 m at nadir and pixels are aggregated into boxes of 10 $\times$ 10 pixels in order to derive the aerosol parameters on a scale of 0.5 $\times$ 0.5 km^2. The cloud mask algorithm [*Ackerman et al.*, 1998] is applied to each pixel in the box and if the number of noncloud pixels per box are above a threshold value, the mean radiance of the box is used for retrieval of aerosol properties. The ER-2 usually flew along a "racetrack" pattern over open water, approximately 160 km in length, in which the two legs of the track were separated by 10 km.

[20] Mounted under the wing of the C131 aircraft, the Particle Measuring Systems' (PMS) PCASP-100X was the instrument utilized to measure particle size distributions. The PCASP, which sizes particles between about 0.1 and 3.0 μm (diameter), operated well in TARFOX. Since the deicing heater was always on, the PCASP first dried the particles, then pumped them through the instrument at a constant flow rate of 1.0 cm^3/sec. There are uncertainties associated with conservation of number of particles because the airflow is decelerated and then pumped through the instrument. *Strapp et al.* [1992] have shown these uncertainties to be of minor importance, and they are assumed negligible in this study. However, the instrument was calibrated with glass spheres, and thus will have some uncertainty in the sizing of aerosols due to the difference in refractive indices of this material from the measured aerosols. *Hartley et al.* [2000] found that an adjustment to the bin boundary was necessary in order to achieve closure between Mie-derived scattering coefficients and measured ones. Based on *Hegg et al.* [1997] and *Novakov et al.* [1997] compositional analysis, *Hartley* [2000] determined the mean dry index of refraction of the aerosols studied during TARFOX (1.46-0.0086i) and applied it to obtain the corresponding corrected bin limits for the PCASP.

[21] The aerosol size distributions from the ACE-2 data set are the ambient composite distributions derived from three aerosol sizing instruments [*Collins et al.*, 2000]: differential mobility analyzer (DMA, size range 9–190 nm), PCASP-100X (with deicers off) and the forward scattering spectrometer probe (FSSP-100, size range 0.5–8.0 μm diameter). The combined measurements from the three instruments characterize the size range critical for optical properties. Numerous corrections have to be applied to the raw data as thoroughly discussed by *Collins et al.* [2000]. Furthermore, the FSSP instrument functioned only in the first 9 flights and, thus, was not operational during the flights where dust was sampled. In those cases, *Collins et al.* [2000] extrapolated PCASP size distribution to the coarse mode range. This extrapolation was validated with comparisons of coarse mode measurements made by another aircraft (the Merlin [*Brenguier et al.*, 2000]).

[22] The AATS-14 (Ames Airborne Tracking 14-channel Sunphotometer) was onboard of the Pelican and measures the transmission of the direct solar beam in 14 spectral channels (380 to 1558 nm). AATS-14 is an extended and improved version of the AATS-6 instrument. With the increase in number of bands, the newer instrument has the ability to correct more precisely for the effects of water vapor and ozone. From the measured transmission, the spectral optical depth is derived in 13 bands and total columnar water vapor and ozone. During ACE-2, the AATS-14 acquired data in 14 flights [*Schmid et al.*, 2000]. The uncertainty in optical depths is due to uncertainties in calibration, signal measurement, air mass computation and corrections for molecular scattering and absorption and is computed following *Russell et al.* [1993].

[23] Since the aim of this work is to utilize these in situ data in the derivation of the mse, and since no remote data from MODIS are available in the fields experiments here studied (note that MAS was flown during TARFOX and some limited data is available, see section 4), we derived r_{eff} and η from the in situ data as proxies of the remotely sensed parameters defined by *Tanré et al.* [1997]. The in situ columnar effective radius was derived as the weighted integral of the volume to surface ratio measured in each profile:

$$r_{eff}(column) = \frac{\sum_i r_{\mathrm{eff}}(z_i)\sigma_{sp}(z_i)\Delta z_i}{\sum_i \sigma_{sp}(z_i)\Delta z_i} \tag{9}$$

where the weight $\sigma_{\mathrm{sp}}(z_i)$ is the synthetic aerosol scattering coefficient (from measured distributions) at λ = 0.55 μm at each height z_i.

[24] Similarly, the parameter η was derived as the weighted integral over the column of the ratio of accumu-

lation mode scattering to total scattering derived by Mie calculations:

$$\eta(column) = \frac{\sum_i \eta(z_i)\sigma_{sp}(z_i)\Delta z_i}{\sum_i \sigma_{sp}(z_i)\Delta z_i} \quad (10)$$

where $\eta(z_i)$ is computed at z_i as the ratio of synthetic scattering coefficients computed from the PCASP size distributions for particles below 1 μm diameter and the whole distribution respectively. The wavelength was 0.55 μm and the index of refraction is dictated by the type of aerosol (1.46-0.0086i average value for TARFOX, [*Hartley et al.*, 2000] and 1.54-i0.001 for dust in ACE-2).

2.5. Parameterization of Mass Scattering Efficiency

[25] The MODIS aerosol retrieval algorithm derives the extinction aerosol optical depth in seven bands and, in addition, derives aerosol effective radius (r_{eff}) and the contribution of the accumulation mode to the total radiance in the column [*Tanré et al.*, 1999]:

$$I_{total} = \eta I_{acc} + (1 - \eta) I_{coa} \quad (11)$$

These parameters are representative of columnar properties and they are partially interdependent since they are related to the size distribution. However, r_{eff} depends exclusively on the size distribution whereas η depends also on the composition and wavelength through the efficiency factor.

[26] Interpretation of the meaning of r_{eff} and η as derived by MODIS and how these parameters relate to the actual physical properties under observation have not been clearly assessed. A few studies carried out by researchers in the remote sensing community have analyzed the meaning of optical derived r_{eff} and η. For example, in the MODIS algorithm [*Tanré et al.*, 1999], η is defined as a free parameter that is adjusted such that it minimizes the difference between the measured and the precalculated radiance. It is assumed to be independent of wavelength. Recent studies of inversion aerosol size distributions from sunphotometer data define also a parameter η as a ratio of optical depths at different wavelengths but it has been was applied only to reconstruct the observed spectral dependence of optical depth (Angstrom coefficient) [*O'Neill et al.*, 2001]. In order to be able to compare the AERONET derived η, the next version of the MODIS aerosol algorithm will redefine η as τ_{acc}/τ_{total} (Y. Kaufman, personal communication, 2001). Only a handful of studies have been dedicated to comparing these retrieved properties with in situ measurements. In fact, validation studies of MODIS data with collocated in situ profiles are in progress (ACE-Asia (March 2001), PRIDE (Puerto Rico Dust Experiment, summer, 2000), CLAMS (Chesapeake Lighthouse and Aircraft Measurements for Satellites, summer 2001)). More recently a study by *Remer et al.* [2002] compared sunphotometer retrievals with MODIS derived r_{eff} and determined that MODIS retrievals are within the expected retrievals errors calculated by *Tanré et al.* [1997]. A few studies have been dedicated to the comparison of profiles of in situ data and sunphotometer derived size distributions [*Fouquart et al.*, 1987; *Remer et al.*, 1997; *Reid et al.*, 1999; *Campanelli et al.*, 2001] that showed agreement between columnar retrieved parameters such as r_{eff}, volume and Angstrom coefficient, and in situ measurements. These studies have all in common that the remotely sensed and in situ data compared is representative of measurements taken within only hours with the common assumption that the aerosol layer does not change its properties significantly between the in situ sampling and the remote sensing measurement. Comparisons of aerosol retrievals using measurements that span shorter periods of time are scarce and difficult to achieve. For example, *Gassó and Hegg* [1997] showed a detailed comparison in fresh smoke where the time difference between the remote sensing and in situ measurements was of the order of minutes.

[27] In order to derive a mse customized to the pixel under observation, a parameterization of the scattering efficiency in terms of the quasi-independent variables (r_{eff} and η) has then been derived. Thirty bilognormal size distributions were used along with a Mie code to generate the corresponding mse's. The geometric mode radius (r_g), logarithm of the geometric standard deviation ($\ln(\sigma_g)$) and effective radius (r_{eff}) are the MODIS algorithm size distributions [*Tanré et al.*, 1997]. Three indexes of refraction where assumed with no absorption (n = 1.54-0.0i, 1.45-0.0i and 1.34-0.0i), density (ρ = 1.7 g/cm^3) and different degrees of mixing of the accumulation mode and coarse mode. In order to span a reasonable range of r_{eff} and η, the concentration of both modes was kept constant (N_{accu} = 1000 part/cc and N_{coarse} = 10 part/cc) but the contribution of each mode to the total volume was varied such that $V_{tot} = E * V_{acc} + (1 - E) * V_{coa}$ where $0 < E < 1$. A few test runs with 10 values of E for each of the bilognormal distribution spanned all values of η and the r_{eff} of the resulting distributions ranged from 0.05 to 5.5 μm. For the Mie computations, η was computed as $\eta = \sigma_{sp,small}/(\sigma_{sp,small} + \sigma_{sp,large})$ at λ = 0.55 μm (small and large are the labels defined in *Tanré et al.* [1997] for accumulation and coarse modes). The effective radius was computed as the ratio of the third and second moment of the bilognormal distribution. The bilognormal distributions combined each of the coarse mode distributions with each of the accumulation mode distributions (30 combinations). The mass scattering efficiency was computed as the ratio of the scattering coefficient divided by the amount of mass contained in a unit volume of air at $\lambda = 0.55$ μm. Particles were assumed to be spherical and internally mixed.

[28] The variable domain generated by the Mie code is shown in Figure 1 and illustrates the relationship between the mass scattering efficiency (α) and the two selected predictors. It is clear that the dominant presence of large particles (high r_{eff}) results in a small mse regardless the composition. However, when there is a significant contribution of accumulation mode particles ($\eta > 0.6$), mse is more dependent on composition and the number of coarse mode particles in the active optical region. The dependency of mse as a function of η indicates that when the contribution of the accumulation mode is small or moderate, mse is fairly constant and independent on composition. A nonlinear fit was derived to relate η and r_{eff} to α for the three different indexes of refraction:

$$\alpha(\eta, r_{eff}) = 0.1 + 2 * \exp\left[-\frac{(r_{eff} - c_1)^2}{c_2} - \frac{c_3}{r_{eff}}\right] * \exp\left(c_4 * \eta^2\right) \quad (12)$$

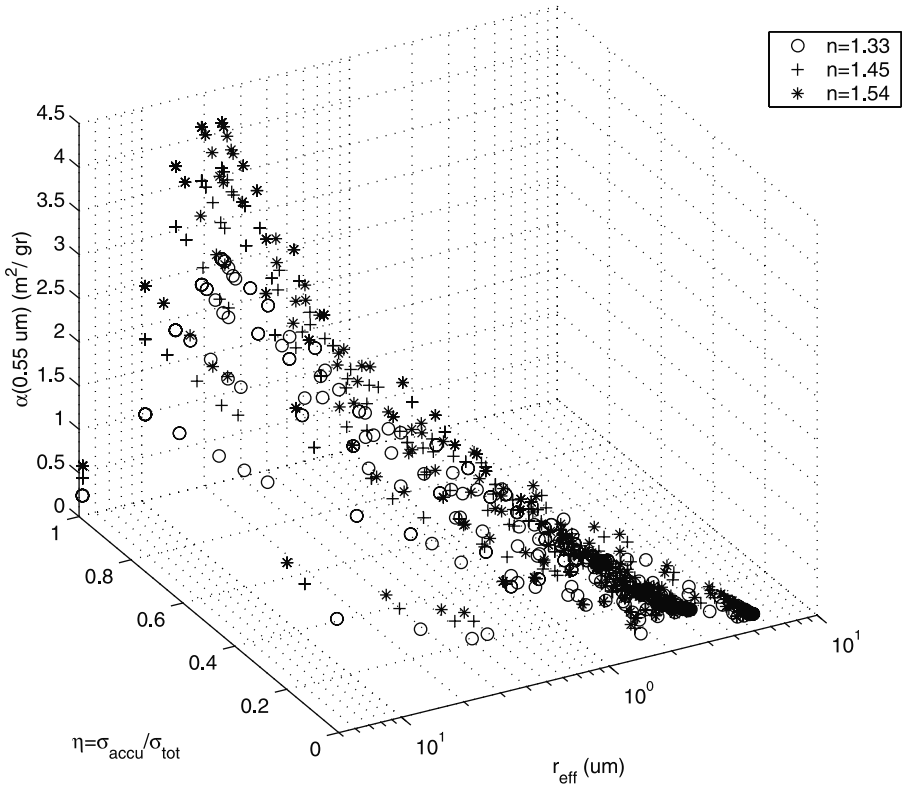

Figure 1. Computed mse at $\lambda = 0.55$ μm for 3 indexes of refraction ($n_{img} = 0.0$) and assumed density of 1.7 g/cm^3 as a function of r_{eff} and η.

where r_{eff} is in μm, α is in m^2/g and the constants are given in Table 1.

3. Retrievals of Aerosol Mass

[29] In this section, we show retrievals of aerosol mass from measurements of aerosol optical depth and compare with simultaneous measurements of aerosol volume derived from in situ size distributions.

[30] The error apportionment indicated by equation (7) suggests that, in conditions of low ambient humidity, the uncertainty in the retrieved mass is reduced. In dry ambient conditions, the factor F(RH, RH$_o$, γ) in equation (6) is near unity and the corrections to the other factors in the equation are minimal. Hence a first test of the value of equation (6) to remote retrievals of aerosol mass is applied to dust measurements.

3.1. Retrieval of Aerosol Mass in Dry Ambient Conditions

[31] The data selected for comparisons are from two flights during ACE-2 where the Pelican encountered dust. These measurements were made in the free troposphere during Pelican flights 15 (8 July) and 20 (17 July) (Figures 2a and 2b, top panels) and exhibited low levels of ambient humidity [*Collins et al.*, 2000]. The thickness of the layers sampled ranged from 0.7 to 1.3 km. Hence, although the optical particle counters operated on the Pelican were running without the heaters on, which implies that particles entering the OPC went through only modest drying (1–2°C) [*Collins et al.*, 2000], the known low hygroscopicity of dust implies that, no correction to ambient conditions was necessary.

[32] In each profile, the mean in situ aerosol volume (V_{true}) was computed by converting the measured number distributions into volume distributions. Then an average over the layer was computed and multiplied by the column thickness. Since the distributions reported by *Collins et al.* [2000] are a combination of distributions from different instruments and no uncertainties were reported in their data, the error in V_{true} was computed by assuming that the error in each bin is proportional to the square root of the counts (Poisson statics). This results in an uncertainty equal to:

$$\delta V_{\text{in-situ}}(z) = \sum_{i=1}^{15} \delta n_i(z) \frac{1}{6} \pi D_i^3$$

where D_i is the mean geometric diameter of each of the 15 bins and $\delta n_i(z)$ is the uncertainty due to counting statistics ($\delta n_i = n_i^{1/2}$).

[33] The retrieved volume (V_{ret}) was calculated by applying equation (3) (Fraser method) and using the following assumed parameters: i) Dust mass scattering efficiency of

Table 1. Coefficients of the Fit of equation 12

Refractive Index	c_1	c_2	c_3	c_4
1.34-i0.0	0.050	0.977	0.187	1.015
1.45-i0.0	0.050	0.918	0.131	1.215
1.54-i0.0	0.010	1.041	0.108	1.293

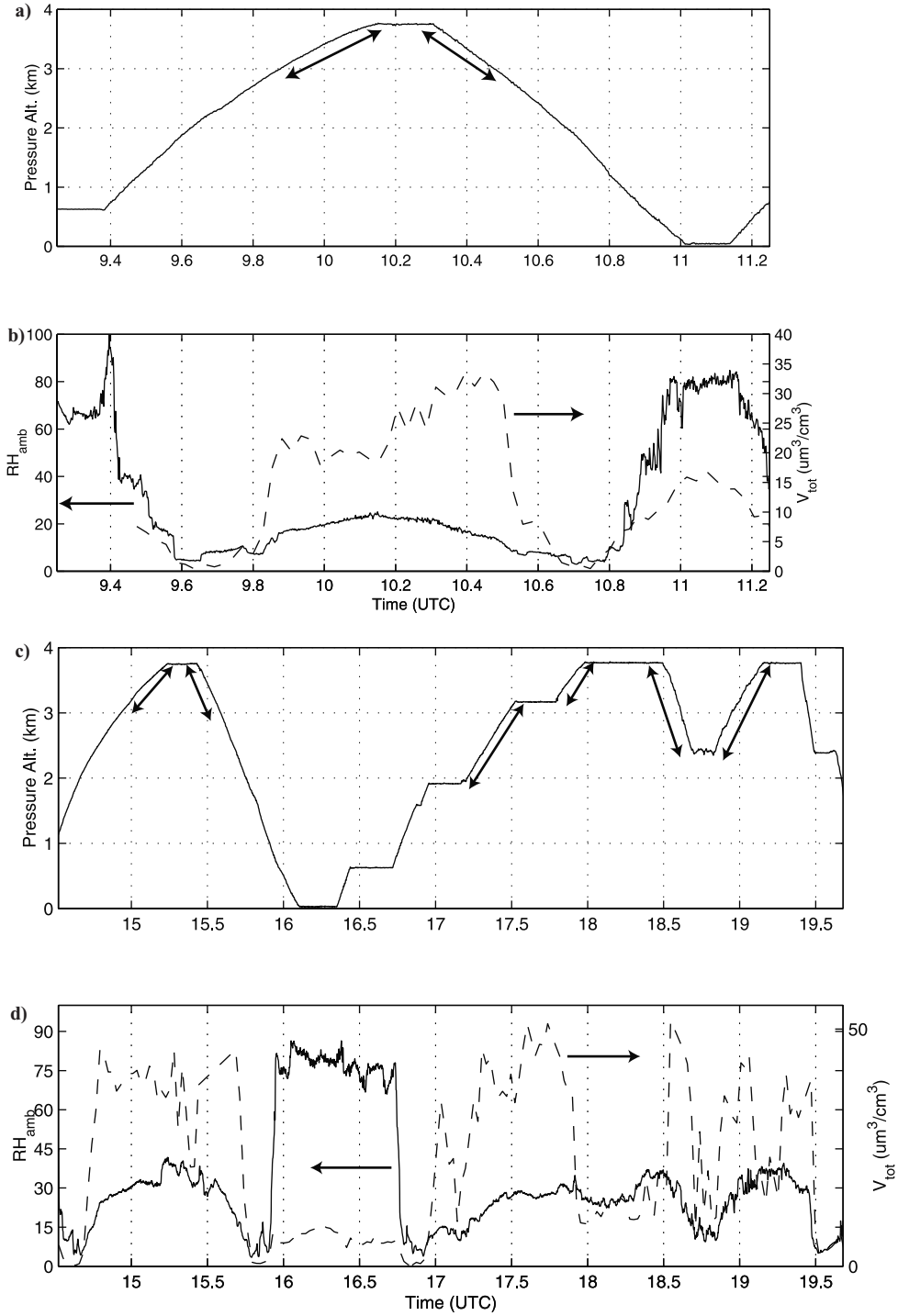

Figure 2. Flight 15 during ACE-2. (a) Altitude of aircraft, the profiles used for retrievals are indicated by the arrows. (b) Ambient RH (solid line) and Total Volume (dashed line). (c) Flight 20 during ACE-2: Altitude of aircraft, the profiles used for retrievals are indicated by the arrows. (d) Ambient RH (solid line) and Total Volume (dashed line).

0.4 m^2/g with uncertainty of 0.3 m^2/g [*Carlson and Caverly*, 1977] ii) Dust single scattering albedo of 0.8 with an uncertainty of 0.2 [*Öström and Noone*, 2000] iii) Dust density of 2.5 g/cm^3 with an uncertainty of 0.5 g/cm^3 [*Fraser*, 1976; *Clarke et al.*, 1996]

[34] References available with measurements of mse for Saharan dust [*Li-Jones et al.*, 1998; *Maring et al.*, 2000] indicate that it can be quite variable (0.2–1.0 m^2/g). Thus, the uncertainty used in the retrieval is based on the variability of mse reported in these studies rather than an actual measured variability. The uncertainty in the density was chosen in a similar fashion. Note that in order to determine the error in V_{ret}, the corresponding uncertainty term in density was included in equation (7). In the case of the

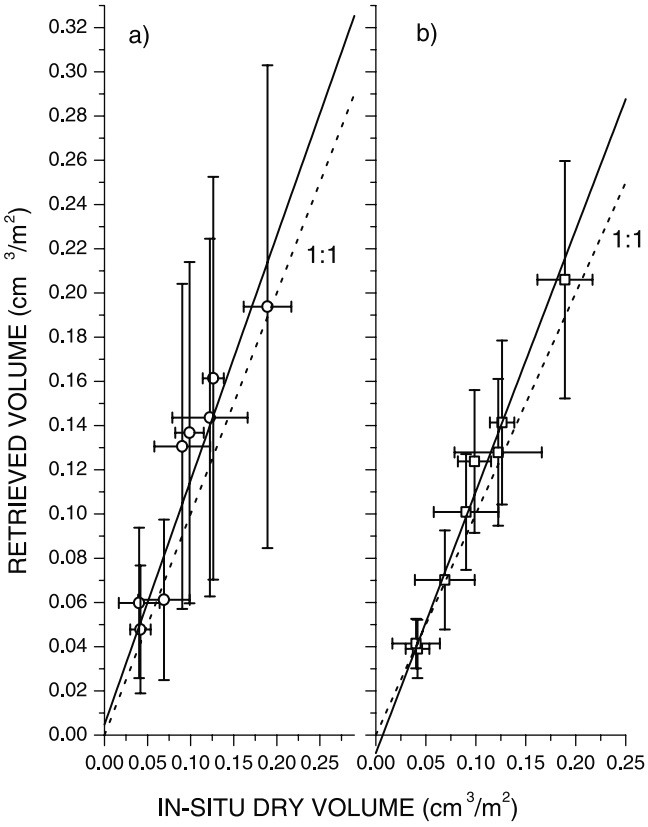

Figure 3. Retrieved Volume (V_{ret}) using different retrieval methods versus In situ derived dry volume ($V_{in\ situ}$) for dust. Best fit (solid line) and one to one line (dash). Panel A: retrieved volume using the Fraser method. Panel B: Retrieved aerosol volume using mse derived from r_{eff} and η.

single scattering albedo, we used the values derived during ACE-2 from measurements taken onboard the Pelican [*Öström and Noone*, 2000].

[35] The retrieved and in situ volumes are displayed in Figure 3a and Table 2. A Pearson ordinary least squares regression yielded a high r^2 of 0.86, a slope of 1.105 (± 0.519) and a zero bias of 0.005 (± 0.036). When considering the uncertainty in the retrieval, the bias is well within the error measurement. As a test, we applied a humidity correction by using the mean measured RH and an assumed γ (= 0.12); the correlation does not change significantly. This is reasonable because of the low ambient humidity (all measurements were made in a dry FT) and low hygroscopicity of the dust.

[36] Table 2 shows that there is a significant contribution of the coarse mode to the total volume (more than 90% in all cases). Also, note that the magnitude of the coarse mode volume and the poor statistics in the OPC for large particles results in a large contribution of the coarse mode error to the total error. As a reference and for comparison purposes with in situ measurements of mass, Table 2 includes the mass concentration equivalent to the $V_{in\ situ}$ for the respective layer assuming an aerosol density of 2.5 g/cm^3.

[37] If the integrated volume is used, instead of the average volume, divided by the layer thickness as V_{true} in the fit, the parameters of the fit remain practically unchanged (slope = 1.059). This is because the plane sampled a relatively homogenous layer and descended at constant speed.

[38] There are no filter measurements available for these dust layers. However, comparison with published literature on Saharan dust reveal that our derived mass concentrations are clearly within reasonable ranges [*Campanelli et al.*, 2001; *Li-Jones et al*, 1998]. Figure 3a demonstrates that an estimation of mean columnar mass (i.e., retrieved volume times assumed density) can be obtained just by assuming reasonable estimations of the parameters involved (the Fraser method). However, as noted above in an operational satellite retrieval there is rarely a priori information on the aerosol event under observation and thus, there is no reason to prefer a particular mse for application of equation (3). Given that, with MODIS, estimations of r_{eff} and η are derivable, we apply the parameterization developed in section 2.5 to obtain an improved estimation of the mse in each pixel. We use in situ derived r_{eff} and η as entry values in formula (12). In this case, we defined η as in equation (10) using the measured distributions with an index of refraction of 1.54-i0.001 and r_{eff} computed from equation (9) (see Table 2). The assumed index of refraction used as an entry value in equation (9) was 1.54. Figure 3b displays the retrieved volume using the parameterized mse.

[39] The parameters of the fit are as follows: the slope is 1.184 (± 0.294) and the intercept = 0.008 (± 0.023) with r^2 = 0.99. The improvement in the correlation indicates that by choosing a mse that it is customized to the scene under observation, the V_{ret} is only slightly improved. However, note in Table 2 that the data utilized for the fit spans a very limited range of r_{eff} (0.88–1.08 μm) and η (0.27–0.33) which resulted in mse's in the range of 0.38–0.42 m^2/g, i.e.,

Table 2. In Situ (Including Accumulation Mode Contribution) and Retrieved Aerosol Volume With Respective Uncertainties[a]

$V_{in\ situ}$, cm^3/m^2	$\Delta V_{in\ situ}$, cm^3/m^2	$V_{in\ situ\text{-}acc}$, cm^3/m^2	$\Delta V_{in\ situ\text{-}acc}$, cm^3/m^2	V_{ret}, cm^3/m^2	ΔV_{ret}, cm^3/m^2	Mass, μg/m^3	r_{eff}, μm	η
0.0417	0.0119	0.0034	0.0005	0.0478	0.0289	66.1	0.9445	0.3061
0.069	0.0299	0.0045	0.0007	0.0612	0.0363	94.2	1.0598	0.2717
0.1263	0.0122	0.0109	0.0007	0.1614	0.0911	135.5	0.9715	0.3203
0.1892	0.0276	0.0135	0.0009	0.1938	0.1092	194.1	1.0345	0.2852
0.0987	0.0166	0.0079	0.0008	0.1368	0.0772	125.9	0.9801	0.303
0.0403	0.0237	0.0036	0.0007	0.0598	0.034	102.9	0.8889	0.3289
0.1224	0.0437	0.0095	0.0013	0.1436	0.0809	141.6	0.9736	0.2981
0.0903	0.0324	0.0081	0.0013	0.1306	0.0735	106.1	0.9276	0.3263

[a] r_{eff} and η are the effective radius and the ratio of $\sigma_{accu}/\sigma_{tot}$ averaged over the column (computed from measured distributions with a Mie code for n = 1.54-i0.001 and λ = 0.55 μm). Mass (μg/m^3) is the equivalent mass concentration corresponding to $V_{in\ situ}$ for an assumed ρ = 2.5 g/cm^3 and respective layer thickness.

very close to the constant value used in Figure 3a. Also, if the assumed index of refraction in the parameterization had been lower, for example 1.43, the resulting range of mse would be 0.22–0.35 m^2/g which results in a change of slope (an increase, in this case) but the correlation remains unchanged.

[40] This suggests that the use of a customized mse in the pixel under observation potentially much improves the accuracy of the retrieval. However, the degree of accuracy is dependent on the index of refraction used in the parameterization. Obviously, a previous knowledge of the aerosol type under observation will help to constrain the retrieval. The validity of this method needs to be further explored with measured data that spans the natural range of variability of r_{eff} and η.

[41] In the next section, data that spans a different range of r_{eff} and η will be studied under conditions of high ambient humidity.

3.2. Retrievals of Aerosol Mass in High-Humidity Conditions

[42] The most common scenario in the marine environment is the one of high humidity in the boundary layer. Also, it is in the boundary layer where most of the aerosol extinction occurs. In this section, we apply equation (6) to the retrieval of aerosol volume where the ambient humidity is high (RH_{amb} > 50%). In this case, we utilized data from the TARFOX campaign.

[43] During TARFOX, the UW aircraft acquired in 20 profiles. The criterion for selecting the data was based on the variability of sunphotometer optical depth (τ_{sunp}) when the plane changed altitude by more than 0.5 km. The τ_{sunp} of the layer was derived by taking the difference between the τ_{sunp}'s at the beginning and end of the profile. As was pointed out by *Russell et al.* [1999], there were cases were the optical depth increased as the plane ascended during the profile. No clear justification exists for such behavior but the most plausible reasons are either the presence of thin cirrus aloft or a change of aerosol mass above the plane. It is assumed that these effects can be removed by taking the difference between τ_{sunp}'s at the top and bottom of the layer. In this study, the PCASP size distributions were adjusted; calibration obtained by *Hartley et al.* [2000] is used. The uncertainty in the total volume at each point of the column ($\delta V_{in\ situ}(z)$) was computed from the propagation of error in the counting statistics of the OPC. All in situ data utilized in validating equation (6) were corrected to the PCASP relative humidity (RH_{pc}).

[44] First, the retrieved dry volume was computed by applying the Fraser method, i.e., by assuming all the parameters in equation (6) but the optical depth. The magnitude of the parameters chosen have been reported in previous TARFOX studies: i) Mass scattering efficiency of 2.8 m^2/g with an uncertainty of 0.3 m^2/g (e% = 100*uncertainty/value = 15%) [*Hegg et al.*, 1997] ii) Single scattering albedo of 0.95 with an uncertainty of 0.03 (e% = 9.97) [*Hartley et al.*, 2000] iii) Density of 2.0 g/cm^3 with an uncertainty of 0.3 g/cm^3 (e% = 15) [*Hegg et al.*, 1997] iv) Aerosol hygroscopic γ exponent of 0.6 with an uncertainty of 0.1 (e% = 17) (based on *Kotchenruther et al.* [1999]) v) Constant ambient RH = (69.1 ± 17.5)% and a reference RH = 30 ± 7.5 % (mean and standard deviation of ambient RH and PCASP RH for all profiles).

[45] The values of mse, ρ and ω_o listed above were reported at dry conditions (below 40%). The uncertainty in the retrieved volume is computed by applying equation (7).

[46] Second, the retrieval of dry volume was attempted by considering the impact of using an $F(RH, RH_o, \gamma)$ and mse customized to the case under observation. For example, in each profile, an estimated mse can be obtained by using equation (12) and an estimation of mean RH in the column. Two retrievals were attempted with customized parameters, one where the hygroscopic exponent (γ) was assumed constant and another where it was assumed variable. The constant γ was equal to 0.6 (± 0.1) and a variable γ was obtained in each profile from the measured hygroscopicity available in each flight [*Kotchenruther et al.*, 1999]. Note that the Kotchenruther et al. study determined the ratio $f(80\%) = \sigma_{sp}(RH = 80\%)/\sigma_{sp}(RH = 30\%)$ at specific altitudes. For this study, γ was derived from the Kotchenruther et al. measurements as $\gamma = -\log(f(80\%))/\log((1-80\%)/(1-30\%))$ and when multiple measurements of f(80%) were available in the same flight, the one closest to the boundary layer was chosen.

[47] Since no MODIS measurements were available for this experiment, we utilized the in situ integrated and scattering weighted r_{eff} and η defined by equations (9) and (10) respectively. The mse used in the volume derivation and its uncertainty were obtained by considering the uncertainties in r_{eff} and η as estimated by *Tanré et al.* [1999]:

$$\alpha_1 = \Phi(r_{eff}*0.75, \eta*0.5) \quad \alpha_2 = \Phi(r_{eff}*1.25, \eta*1.5)$$
$$\alpha = (\alpha_1 + \alpha_2)*0.5 \qquad \delta\alpha = \mathrm{abs}(\alpha_1 - \alpha_2)$$

where Φ is given by equation (12) and $\delta\alpha$ is the uncertainty in α. The index of refraction used in equation (12) is 1.43-i0.0. If a different index is used, the mean mse value does not change significantly because of the range of variability assumed in r_{eff} and η.

[48] In this case, the average RH_{amb} in the factor $F(RH_{amb}, RH_{pc}, \gamma)$ was estimated from the in situ measurements as the average ambient RH and the uncertainty was estimated as the standard deviation over the column.

[49] Figure 4 displays the retrieved volume following the Fraser method (Panel a) and the retrieved volume utilizing a variable mse with variable RH and γ (Panel b) with respective regression fits (solid line). Note that in contrast to the dust case of section 3.1, the magnitude of the derived volumes are about one order of magnitude smaller, that is, they have equivalent mass concentrations in the 6–50 $\mu g/m^3$ range (for an assumed ρ = 1.7 g/cm^3 and Δz = 1 km), consistent with the ranges found in the *Hegg et al.* [1997] study.

[50] Table 3 displays the parameters of the fit including the case of variable mse and rh with constant γ. In this case, the correlation coefficient indicates that the new method does not improve the retrieval significantly as it did with the dust case. However, it is interesting to note that if one applies the Fraser method with the addition of a variable mse (and constant $F(RH_{amb}, RH_o, \gamma)$), the r^2 is 0.61. Moreover, if the Fraser method is applied with a variable $F(RH_{amb}, \gamma$ = constant) and constant mse, the corresponding

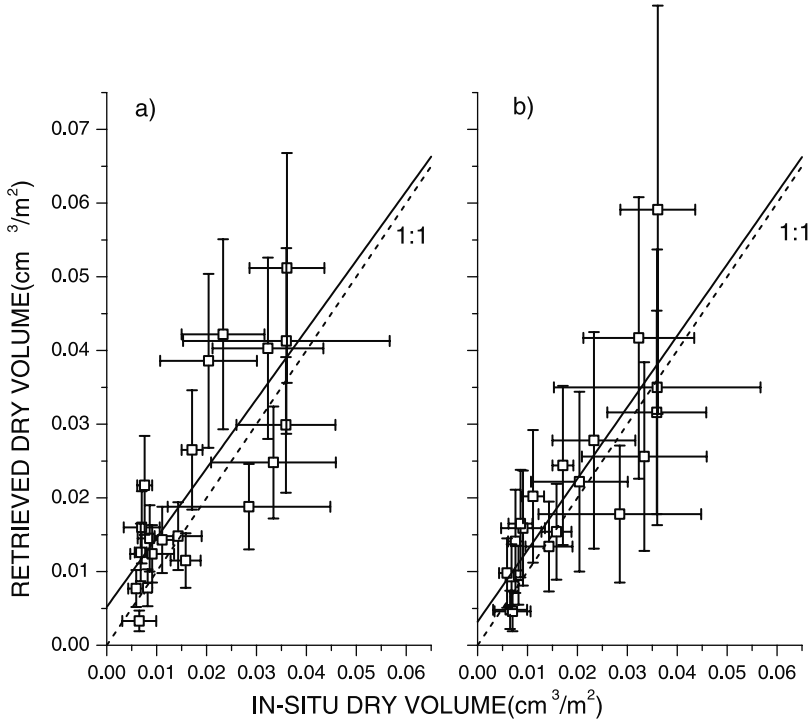

Figure 4. Retrieved Columnar dry values (V_{ret}) using the Fraser method (constant RH and mse, panel a) and using adjustable mse, RH and γ (panel b) versus $V_{in\ situ}$. Solid line is the fit to the data and dashed line is the one to one line.

r^2 is 0.54. In contrast, when retrieving V_{ret} with both variable mse and F(RH_{amb}, RH_{pc}, γ), the resulting r^2 is 0.70. This suggests that the retrieval is improved by the combined customized parameters compared to the use of just one of the customized parameters.

[51] The lack of significant improvement in the new method is not surprising and we can distinguish two issues that may justify why there is no significant improvement: precision of the data used and the quality of the method in retrieving the columnar volume. As was mentioned before, the adjustment of in situ data to ambient conditions requires a number of corrections that may lead to errors, such as the assumed composition of the particles and specifically, the hygroscopicity. Among the in situ measurements, it is possible that the optical particle counter used (PCASP-100) is not measuring all particles. This is suggested by the positive bias (i.e., nonzero ordinate) in the fits shown in Figure 4. Also, if a mse is derived from equation (6) using $V_{in\ situ}$ instead of V_{ret} (i.e., mse = $\tau_{ext}*\omega_o/(V_{in\ situ}*\rho*FRH)$), the derived mse <1.0 m^2/g which is not realistic for the aerosol type studied here. Indeed, the *Hartley et al.* [2000] study concluded that two of the possible problems in comparing synthetic scattering coefficients derived from measured dry distributions with measured scattering coefficients are, an incorrect assumed hygroscopicity and particles not sampled by the OPC. Also, the *Hartley et al.* [2000] study found that in comparing integrated measured scattering coefficients (corrected to ambient conditions) with measured optical depths, the in situ measurements consistently underestimated (by 10% on average) the sunphotometer measurement. So, there are indications that the in situ sampling biases and the correction to ambient conditions are important when comparing columnar measurements of aerosol volume. The selection of the PCASP calibration also clearly plays a role in retrieval accuracy because, in comparing the V_{ret} with $V_{in\ situ}$ derived with the factory calibration (1.53-i0.0), the bias and the slope of the fit are both about 50% larger.

[52] Finally, it is possible that the magnitudes of the optical depths are not correct. It was assumed that the aerosol layer in the column remained unchanged during the profile. As was suggested by *Hartley et al.* [2000] and verified later by the Ames research group in charge of the photometer (NASA Ames group, J. Livingston personal communication, 2000), it was possible that cirrus clouds or aerosol layers unsampled by the plane moved into the field of view of the sunphotometer while the profile was being obtained.

[53] With respect to the new method, it is possible that a correction with a constant F(RH_{amb}, RH_{pc}, γ) is not sufficient to correct the ambient optical depth to dry conditions. That is, the nonlinear effect of aerosol hygroscopicity on the optical properties cannot be accounted for by the simple correction proposed here. Specifically, the implicit assump-

Table 3. Parameters of the Fit to $V_{in\ situ}$ versus V_{ret} for Using Different Assumptions (See Text)

No.		Slope (± Error)	Ordinate (± Error)	r^2
1	Fraser method	0.948 (0.171)	0.00526 (0.00365)	0.63
2	Variable mse, RH_{amb} and constant γ	1.016 (0.160)	0.00369 (0.00342)	0.69
3	Variable mse, RH_{amb} and γ	0.973 (0.149)	0.00324 (0.00318)	0.70

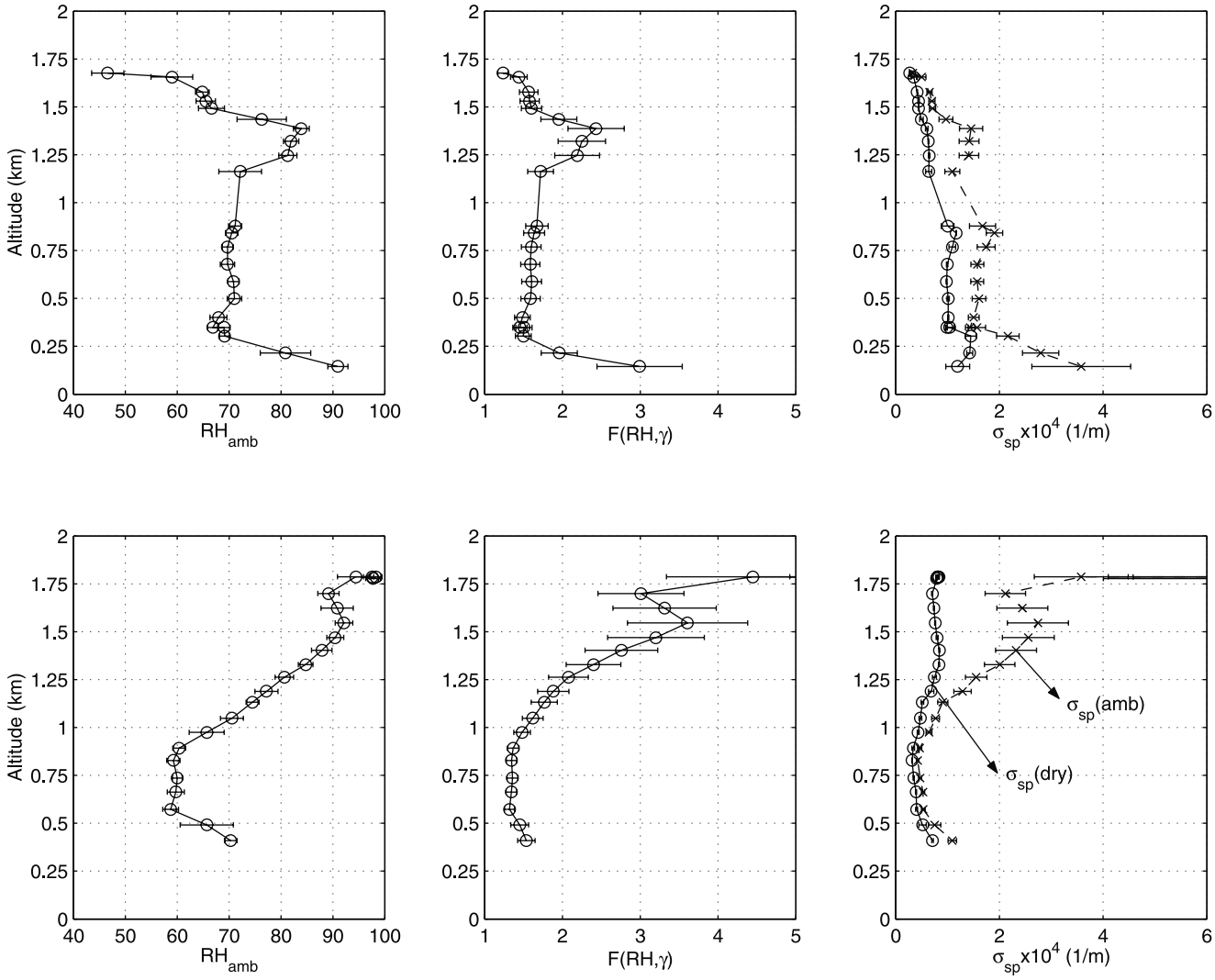

Figure 5. Profiles of RH_{amb}, $f(RH_{amb},\gamma) = (1 - RH_{amb}/1 - RH_{neph})^{-\gamma}$ (γ derived from the respective flight) and measured dry σ_{sp}(neph) and derived σ_{sp}(amb) for profiles taken during flights 1724 (bottom row) and 1728 (top row).

tion in using equation (6) to correct the optical depth is that RH and γ are constant throughout the column and certainly this will not always be true. For example, Figure 5 shows profiles of RH_{amb}, $F(RH_{amb}, RH_{neph}, \gamma) = (1 - RH_{amb}/1 - RH_{neph})^{-\gamma}$ and measured dry σ_{sp}(neph) and derived σ_{sp}(amb) for profiles taken during flights 1724 (bottom row) and 1728 (top row). Flight 1728 shows a fairly constant humidity profile with two layers ($\sim$0.25 km thickness each) above 75% RH. σ_{sp}(amb) is decreasing with altitude and follows approximately an exponential function in the bottom of the profile. It is significantly higher than σ_{sp}(dry) in the bottom layer. Flight 1724 shows a case of high levels of RH aloft in an extended layer ($\sim$0.8 km thickness) and the corrected σ_{sp}(amb) are significantly higher. Table 4 shows the derived optical depth computed from the two flights using different methods. In Table 4, Δz is the difference between the top and bottom of the profile and the parameters in brackets are the respective mean values over the column. It is clear that in the case of flight 1724, the discrepancies between the integrated scattering coefficients and the mean values are large, whereas in the case of flight 1728 the differences are low (particularly in Case #2, which is essentially equation (2)). These examples show that in cases where the humidity profile is highly variable within the range 80–99% RH in a relatively thick aerosol layer, the corresponding σ_{sp}(amb) cannot be approximated well by its average value due the high sensitivity of scattering to relative humidity in this range. In contrast, when the humidity profile is approximately constant with RH's below 80%, $\int\sigma_{sp}(amb, z)dz$ is well approximated by the product $\langle\sigma_{sp}(dry, z)\rangle$. $\langle F(RH_{amb}(z), RH_o(z), \gamma)\rangle$ even when small layers of high RH (>80%) are present.

[54] Thus, the use of average values of optical properties fails in reproducing integral ambient values when extended and variable high humidity levels collocated with high aerosol concentrations are present in the column.

[55] In summary, the analysis in this section suggests that the retrieval of aerosol mass under conditions of high humidities can be achieved only relatively crudely by the Fraser method. The average error in the cases listed in

Table 4. Ambient Optical Depth Computed by Three Methods for the Profiles Displayed in Figure 5[a]

No.		Flight 1728	Flight 1724
1	$\int \sigma_{sp}(dry,z).\ F(RH_{amb}(z),\gamma)\ dz$	0.231	0.191
2	$\langle\sigma_{sp}(dry,z)\rangle.\langle F(RH_{amb}(z),\gamma)\rangle.\Delta z$	0.234	0.274
3	$\langle\sigma_{sp}(dry,z).\ F(RH_{amb}(z),\gamma)\rangle.\Delta z$	0.232	0.312

[a]The brackets are the average operator applied to the respective quantity.

Table 2 is 50% but the error in individual cases can go up as high as 130%. The use of the same retrieval technique using parameters customized (i.e., mass scattering efficiency and humidity correction) to the scene under observation did not improve the retrieval as much as was the case with Saharan dust. The mean error was 61% with individual cases going up to 180%. When high levels of humidity are present, the new method seems to better predict aerosol mass than the Fraser method, as is indicated by the slight improvement in the correlation coefficient. However, the analysis presented does not clearly indicate that the addition of a variable humidity correction improves the retrieval significantly.

4. Two Case Studies of Retrievals of Aerosol Properties

[56] While useful, the above analysis is not a validation of the method. A proper validation requires comparisons with data obtained from a spaceborne platform with simultaneous measurements in situ. There are very few data sets available where such comparisons can be performed. Field campaigns specially devised to compare satellite or an airborne satellite prototype measurements with in situ platforms are extremely difficult to implement. For example, during TARFOX there were only four instances where the ER-2 flew while the C131 plane was profiling the same volume scanned by MAS. Furthermore, only two of the four flights are suitable (see below) for comparisons. In this section, we use the MAS data from those two flights and compare with in situ data. Our goal is to show the difficulty of performing a comparison of retrieved aerosol properties with the actual aerosol properties derived from in situ data. However, we also show that even when not all the ostensibly necessary information is available such a comparison can be made.

4.1. Coordinated Flights During TARFOX

[57] In the following analysis, the same cases studied by *Tanré et al.* [1999] are revisited. The same algorithm was used with one important modification. After the publication of *Tanré et al.* [1999], the MODIS team found that the glint rejection angle (i.e., the threshold angle below which pixels are influenced by solar specular reflection) in the MAS algorithm was too low and it resulted in spurious optical depths (see, e.g., Plate 2 in the work of *Tanré et al.* [1999]). Thus, the algorithm was modified by increasing the threshold angle (from 30° to 40°) and this is the version used in this study. The main consequence of the change in angles is the significant reduction in the number of pixels available for retrieval. The aerosol retrieval algorithm was developed by *Tanré et al.* [1997] and tested in several field experiments [*Gassó and Hegg*, 1997; *Chu et al.*, 1998; *Tanré et al.*, 1999].

[58] The ER-2 flew on nine days in TARFOX and four of them in coordination with the UW C131 (17, 20, 24, and 25 July). Out of the four cases, two cases (17 and 24 July 1996) were selected for comparison with in situ data measured by the C131. The 20 July case was not selected because it was a very clean day with low optical depths and the in situ instrumentation was operating near noise level. In the 25 July case, the C131 flew briefly at constant altitude in the region scanned by MAS nearly synchronous in time but most of the C131 transect is in the glint of the picture. Also, the C131 did not profile the column in the vicinity of the ER-2.

[59] Of the two cases left, neither of them are "perfect" cases and they illustrate the difficulty of coordinating such comparison experiments. In the case of 17 July, there was good coordination between the aircrafts. However, in the processing of the MAS data, it became clear that the C131 was in the Sun glint while doing the profile. So, in order to compare in situ data with data retrieved from MAS, the pixels adjacent to the profile were used. In the case of 24 July, there was good coordination between the two aircraft and the C131 is in the picture while doing a profile. However, the C131 was not profiling for the specific purpose of comparing with MAS retrievals. As a result, the in situ data in the profile were gathered in a period of ~10 min (compared to a regular planned profile which takes about 20–40 min) resulting in a greater uncertainty in the in situ data due to the shorter time spent in each layer in the column.

[60] Unfortunately, no retrievals of water vapor profiles were available from MAS during TARFOX. Thus, the mean average RH in the column derived from the in situ profile was used.

[61] There is one last element for which it is difficult to account. Because the ER-2 flies at an altitude of 20 km, the size of the boxes (groups of 10 × 10 pixels = 0.5 × 0.5 km) selected for retrievals are smaller than the size of a complete 360° turn of the C131 when doing a profile. This results in an in situ measurement which is representative of different boxes at different altitudes. We will later discuss how we dealt with these issues. However, note that this problem arises only in a situation like this where the detector is at low altitude. In a validation study with coordinated measurements made by plane and the actual satellite, the size of the boxes is 10 × 10 km.

[62] Finally, an extra aerosol parameter is computed from the remotely sensed data and compared with in situ measurements. The parameter is the columnar CCN concentration. Cloud Condensation Nuclei active at supersaturations characteristic of marine stratocumulus (the clouds most important from the standpoint of indirect forcing) would have dry diameters of the order of 0.1 μm or larger (corresponding to ~0.2% supersaturation [*Fitzgerald*, 1973]). This size range most closely corresponds to that measured by the PCASP-100X instrument and it is easily obtained from in situ measurements. The remotely derived CCN concentration is computed by three different methods. One is the standard operational output of the MODIS aerosol algorithm. It is calculated by integration of the accumulation mode size distribution found by the MODIS algorithm [*Tanré et al.*, 1997, Appendix A]. This distribution is obtained from the modeled radiance that best

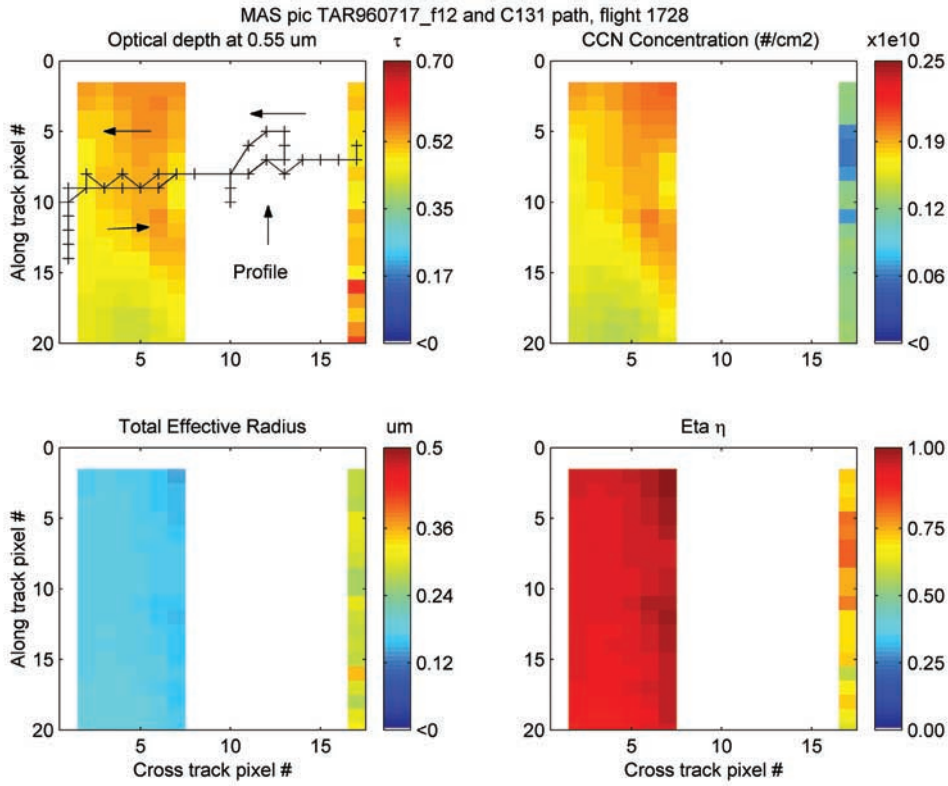

Figure 6. Parameters derived by MAS (track 08) during C131 flight 1728. Retrieved parameters by MAS. τ(0.55 μm) (upper left including C131 track), CCN concentration ($\times$ 10^{10}) (upper right), r_{eff} (bottom left) and η (bottom right).

matches the observed radiance. The other two derivations are based on the analysis of in situ instrumentation. *Hegg and Kaufman* [1998] and *Hegg and Jonsson* [2000] found that the number-to-volume concentration ratio of a size distribution (between 0.12 and 3.8 μm diameter) can be parameterized according to the aerosol type. *Hegg and Kaufman* [1998] found that the ratio is roughly constant for marine aerosols while the *Hegg and Jonsson* [2000] study suggested that the variability in the ratio can be parameterized as a function of the effective radius (dry conditions):

$$\frac{N}{V} = \frac{0.75}{\pi(1.09 r_{\text{eff}})^3} \tag{13}$$

4.2. Case 17 July 1996, Flight 1728

[63] On 17 July, about one hour of clear-sky data, starting at around 1830 UTC, which corresponded to ER-2 flight tracks 10, 11, and 12 [*Tanré et al.*, 1999]. In the postprocessing of the MAS data with the new glint condition, the pictures taken during tracks 10 and 11 have very few good retrievals, none of them near a region sampled by the C131. Track 12, however, is suitable for a comparison with in situ data. In this case, the C131 was still at a high altitude but had just finished the profile in the glint of track 12. The near surface, constant altitude passes right before the profile are in nonglint boxes. Figure 6 displays the data from track 12 and the respective parameters derived by the MAS algorithm (note the units on the axes refer to pixel number in the along (rows) and cross (columns) track).

[64] The upper left panel of Figure 6 shows the track of the C131 superimposed. Note that for purposes of clarity, only those points that are closest in time to the ER-2 pass are shown in Figure 7. The location and times where the C131 is located in Figure 6 are listed in Table 5.

[65] Table 5 lists the MAS primary products τ, r_{eff} and η, along with the retrieved CCN columnar concentration ($\times$ 10^8 particles/cm^2). Also, the derived mass scattering efficiency from equation (13), retrieved columnar volume derived with the new method and the CCN concentrations derived with constant and variable (i.e., dependent on r_{eff}) N/V ratio are listed. The constant parameters (ρ, ω_o, γ, RH, mse) used in the volume retrievals are those defined in section 3.2. Note that because equation (12) was defined for aerosol in dry conditions, the retrieved MAS r_{eff} has to be corrected. In this case, because no RH estimation is available from MAS, we assumed such a correction from the ratio between the MAS r_{eff} and the in situ dry column average r_{eff} (shown in Table 6). The correction for this flight is 1.25.

[66] In Table 5, note that the optical depth between columns 7 and 2 remains basically unchanged and the same occurs for r_{eff} and η. The retrieved CCN concentration mimics approximately the optical depth since the concentration is essentially proportional to $\tau_{\text{small}}/\sigma_{\text{x,small}}$ (normalized). The aerosol concentration measured by the PCASP instrument between 1819:35 and 1822:05 h UTC (i.e., when

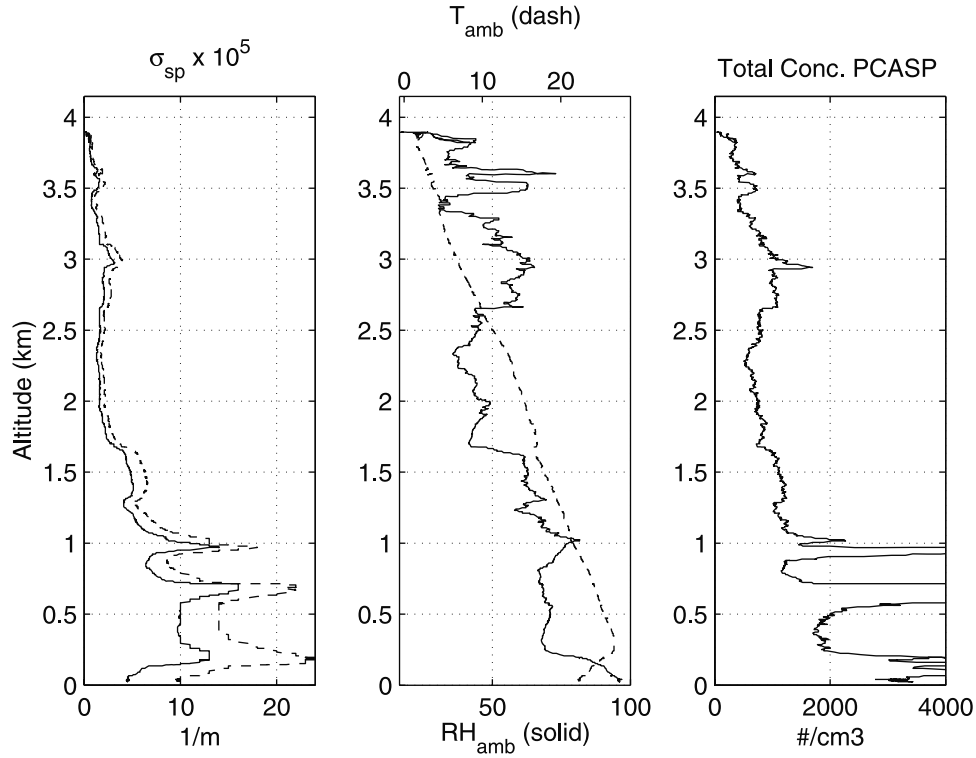

Figure 7. Profile of dry and almost-ambient σ_{sp} (left panel, solid and dash lines respectively), ambient T and RH (center) and total aerosol concentration in flight 1728 used for comparison with MAS data.

the C131 was flying at constant altitude) is rather constant ($\sim$3100 part/cm^3) at 0.2 km altitude. So, the constancy of the optical depths correlates well with the constancy of the aerosol concentration during the low altitude pass and it appears that there is no significant change of aerosol concentration above the C131. The C131 starts a profile at 1830:00 h UTC and we assume that optical depths adjacent to the glint area are the same as the optical depths in the glint.

[67] The data representative of the column measured during the profile are in Table 6 and the profiles of measured scattering coefficient, aerosol concentration, ambient RH and temperature are in Figure 7. Note that in the left hand side panel, data from a nephelometer running at almost ambient condition is shown. The only heating known to be affecting the sample is the heating in the tubing from the inlet to the instrument. Unfortunately, no RH measurements inside the nephelometer are available nor

Table 5. MAS Retrieved Parameters[a] and Derived Columnar Volume[b] and CCN Concentration[c] for Each Pixel Along the Track of the C131 in the Upper Left Panel of Figure 6[d]

C131 Time (h UTC)	Row	Column	τ(0.55)	r_{eff}, μm	η	$\alpha(r_{eff}, \eta)$, m^2/g	V_{ret}, cm^3/m^2	V_{Fraser}, cm^3/m^2	CCN_{ret}, $\times 10^8$ 1/cm^2	CCN_{ret2}, $\times 10^8$ 1/cm^2	CCN_{MAS}, $\times 10^8$ 1/cm^2
1815:50	7	17	0.453	0.29	0.784	2.81	0.045	0.0452	9.0	6.80	6.2
1815:50–1819:35						C131 was in glint of MAS picture					
1819:35	8	7	0.471	0.168	0.933	3.51	0.0375	0.047	7.49	3.01	1.65
1820:00	8	6	0.504	0.17	0.929	3.50	0.0403	0.0503	8.06	2.66	1.76
1820:25	9	5	0.511	0.173	0.921	3.46	0.0413	0.051	8.26	2.68	1.77
1820:50	8	4	0.5	0.176	0.913	3.42	0.0409	0.0499	8.17	2.95	1.71
1821:15	9	3	0.488	0.176	0.912	3.41	0.04	0.0487	7.99	3.09	1.67
1821:40	8	2	0.465	0.175	0.915	3.43	0.0379	0.0464	7.58	3.34	1.61
1822:05	9	2	0.47	0.176	0.913	3.42	0.0384	0.0469	7.68	3.36	1.61
1822:05–1828:45						C131 was in glint and out of MAS picture					
1828:45	9	2	0.47	0.176	0.913	3.43	0.0384	0.0469	7.68	3.32	1.61
1829:10	9	3	0.488	0.176	0.912	3.41	0.04	0.0487	7.99	3.09	1.67
1829:35	9	4	0.494	0.177	0.908	3.39	0.0407	0.0493	8.14	3.09	1.68
1830:00	9	5	0.511	0.173	0.921	3.46	0.0413	0.051	8.26	2.68	1.77
1830:25	9	6	0.505	0.169	0.932	3.51	0.0402	0.0504	8.04	2.62	1.77
1830:50	8	7	0.471	0.168	0.933	3.51	0.0375	0.047	7.49	3.01	1.17

[a]MAS retrieved parameters include τ, r_{eff}, η, and CCN_{MAS}.
[b]Derived columnar volume is expressed as cm^3/m^2.
[c]CCN concentration is expressed as the amount multiplied by 10^8 1/cm^2.
[d]$CCN_{ret} = N/V$ is constant, CCN_{ret2} = the N/V is a function of r_{eff}, and CCN_{MAS} is the standard output from MAS algorithm.

Table 6. In situ Measurement of Several Parameters (Uncertainties in Parentheses) During Flight 1728, Time 1831–1859 h UTC

Parameters	Measured Value	Remark
$V_{\text{in situ}}$, cm^3/m^2	0.0337 (0.0027)	Integrated Dry Volume from the PCASP instrument
RH, %	56.73 (2.12)	Integrated Ambient RH
γ	0.60 (0.1)	Hygroscopicity measurement from *Kotchenruther et al.* [1999] for this flight
FRH(RH, γ)	1.42 (0.09)	Integrated hygroscopic factor (correction from ambient to PCASP RH)
$N_{\text{tot}} \times 10^8$, part/$cm^2$	4.0130 (0.00367) All bins 4.0089 (0.00593) Bins 1–8	Total number of particles in the column (PCASP)
Mass scattering efficiency, m^2/g	3.45 (z = 1 km) 3.55 (z = 0.1 km)	Derived by *Hegg et al.* [1997] in this flight.
Single scattering albedo	0.93 (z = 1 km) 0.97 (z = 0.1 km)	Derived by *Hegg et al.* [1997] in this flight.
Ratio N/V, $1/\mu m^3$	199 (1)	Derived by *Hegg and Kaufman* [1999]
Dry r_{eff}, μm	0.1401 0.1408	= mean($V_{\text{tot}}(z)/S_{\text{tot}}(z)$) = $\int r_{\text{eff}}(z)dz/\Delta z$
Dry η	0.9279 0.8936	= mean($V_{\text{acc}}/V_{\text{tot}}$) = mean($\sigma_{sp}$(accu)/$\sigma_{sp}$(total))
Ambient Temperature	T(z = 0.083 km) = 23.5 T(z = 1.67 6km) = 16.5	Measured at top and bottom of the profile

are possible shifts in calibration documented since the instrument ran automatically throughout the whole experiment (D. Covert, personal communication, 2000). However, it is shown here to give a qualitative idea of the amount of drying in the scattering coefficient.

[68] The retrieved values of columnar volume, which are representative of pixels adjacent to the point where the profile was made, compare reasonably well with the in situ columnar volume. In particular, the volume derived with the new method is somewhat closer to the true value than the volume derived with the Fraser method. With regards to the CCN columnar concentrations, note that all three retrievals are within the same order of magnitude. This is notable given that the concentration is derived from simple relationships. More quantitatively, the constant N/V ratio method is a factor of 2 higher, the MAS derivation is a factor 2.4 smaller and the variable N/V ratio derivation is a factor of 1.2 smaller. Note that given that the in situ measurements do not sample all the particles in the column, whereas the MAS optical depth is sensitive to all particles, it is seems more reasonably to favor the CCN columnar concentration derived with the constant N/V ratio (CCN_{ret}).

[69] For reference, the in situ dry r_{eff} and η (from equations (9) and (10)) are listed in Table 6. Note that r_{eff} is computed by two methods: the ratio of $0.75*V_{\text{tot}}(z)/S_{\text{tot}}(z)$ averaged over the column and as the integration of $r_{\text{eff}}(z)$ over the column. They yield essentially the same result because the constant speed of the plane during the profile. The contribution of the accumulation mode was also computed by two methods: the average ratio of volumes and average of accumulation scattering to total. Note that both computations give similar results. We verified also that the integration of the same parameters over the column are essentially the same as the average η shown in Table 6.

[70] In addition, note that the in situ η compares very well with the retrieved η even though the former is measured in dry conditions, whereas the latter is in ambient conditions. One explanation for this agreement is that the hygroscopic effects cancel out partially when considering the ratio $I_{\text{accumulation}}/I_{\text{total}}$. The in situ effective radius is about a factor 1.25 smaller that the MAS r_{eff}.

4.3. Case 24 July 1996, Flight 1733

[71] A stationary front, orientated east–west and crossing the shoreline over North Carolina, was slowly moving northward, bringing clouds to the observation area and bands of cirrus were quickly moving over the ocean from the continent. We analyzed ER-2 tracks that correspond to the best parts of the flight considering the occurrence of clouds and the presence of Sun glint during the first loops. Track 8 (1902–1911 h UTC) is closest in space to the region sampled by the C131. In this area, the C131 did 3 profiles: 1553–1616, 1740–1753 and 1849–1915 h UTC. The first profile was located just at the edge of the picture (38.8N, −74.25W), the second profile was in the glint area (38.5,−74.3). The third profile is the closest in time to the ER-2 pass and the C131 was in the glint-free region making a low altitude pass. Then it ascended to 2.0 km while in transit (starting at 1849 h UTC and reaching the top at 1914 h UTC, 38.7N, −74.3W). Figure 8 shows the parameters retrieved by MAS with the C131 track superimposed (third profile). The right-to-left arrow in Figure 8 indicates the low altitude pass. After a short banking out of the picture (column 1 in Figure 8), the plane started to go up toward the glint area (in white, Figure 8). Table 7 lists the values of the pixels crossed by the C131 track. Note the variability of the retrieved parameters in the time frame 1857:52–1859:55 h UTC.

[72] The optical depth changes rapidly as it approaches the left edge of the picture. Assuming the variability is real (i.e., they are not effects due to for example the cloud mask or unaccounted glint), the in situ data can provide some insight into possible reasons of this variability. The in situ data from the C131 indicates that the ambient RH ranges over 90–95% and the PCASP concentration ranges 3700–3850 part/cm^3. This suggests that the variability could be

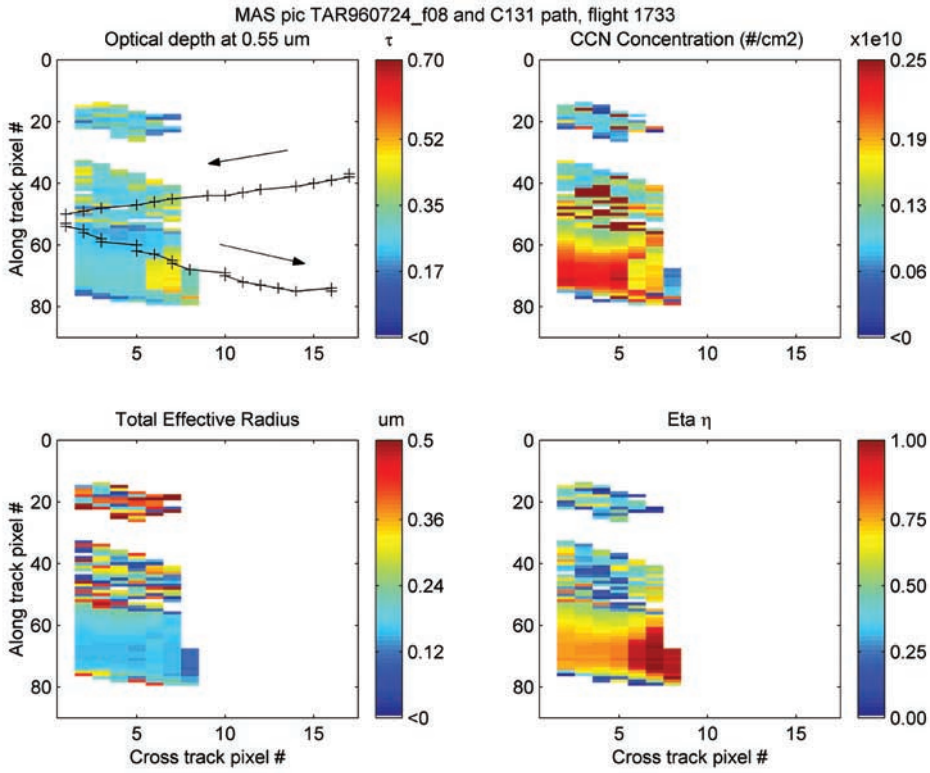

Figure 8. Parameters derived by MAS (track 12) during C131 flight 1733. Retrieved parameters by MAS. τ(0.55 μm) (upper left including C131 track), CCN concentration ($\times$ 10^{10}) (upper right), r_{eff} (bottom left) and η (bottom right).

caused by local variation of ambient RH (remember that scattering is highly variable at these RH's) or the presence of higher (or lower) aerosol concentration above or below the C131. When the C131 starts the profile, it crosses an area of increasing optical depth as it moves toward the glint (starting at 1905:52 h UTC). The fact that retrieved effective radius and η decrease and increase respectively (as seen by the MAS) indicates that the accumulation mode concentration in the column increases.

[73] The in situ data indicates that during the first 500 meters of the profile (which corresponds to the first two crosses in Figure 8, cross track pixels 2 and 3), there is a drop in RH to below 80% and a decrease of particle concentration to $\sim$2000 particles/cm^3. Then, between

Table 7. MAS Retrieved Parameters[a] and Derived Columnar Volume[b] and CCN Concentration[c] for Each Pixel Along the Track of the C131 in the Upper Left Panel of Figure 8[d]

C131 Time (h UTC)	Row	Column	τ(0.55)	r_{eff}, μm	η	$\alpha(r_{\text{eff}}, \eta)$, m^2/g	V_{ret}, cm^3/m^2	V_{Fraser}, cm^3/m^2	CCN_{ret}, $\times$ 10^8 1/cm^2	CCN_{ret2}, $\times$ 10^8 1/cm^2	CCN_{MAS}, $\times$ 10^8 1/cm^2
1857:52	45	7	0.33	0.632	0.381	1.10	0.0839	0.0329	16.79	6.58	13.3
1858:22	46	6	0.298	0.711	0.338	0.89	0.0938	0.0297	18.75	14.11	10.7
1858:52	47	5	0.302	0.576	0.416	1.27	0.0666	0.0301	13.32	5.22	13.3
1859:22	48	3	0.178	0.129	0.188	1.46	0.0342	0.0178	6.83	0.01	74.9
1859:52	49	2	0.481	0.408	0.762	2.46	0.0547	0.048	10.93	3.83	13.8
1859:55–1902:00	C131 is out of the MAS picture										
1902:22	55	2	0.224	0.204	0.566	2.12	0.0296	0.0224	5.92	3.9	13.4
1902:52	56	2	0.224	0.197	0.587	2.16	0.029	0.0224	5.8	3.4	13.9
1903:22	58	3	0.23	0.193	0.599	2.18	0.0295	0.023	5.89	3.1	14.5
1903:52	59	3	0.234	0.186	0.619	2.22	0.0294	0.0234	5.89	2.6	15.3
1904:22	60	5	0.224	0.195	0.593	2.17	0.0289	0.0224	5.77	3.3	14.1
1904:52	62	5	0.246	0.173	0.663	2.32	0.0297	0.0245	5.93	1.8	17.2
1905:22	63	6	0.261	0.156	0.729	2.48	0.0294	0.026	5.89	1.2	20.1
1905:52	65	7	0.435	0.158	0.962	3.66	0.0332	0.0434	6.65	2.7	15.7
1906:22	66	7	0.447	0.153	0.978	3.74	0.0334	0.0446	6.68	2.4	16.4
1906:52	68	8	0.307	0.111	0.956	3.22	0.0267	0.0306	5.33	0.3	31

[a]MAS retrieved parameters include τ, r_{eff}, η, and CCN_{MAS}.
[b]Derived columnar volume is expressed as cm^3/m^2.
[c]CCN concentration is expressed as the amount multiplied by 10^8 1/cm^2.
[d]$\text{CCN}_{\text{ret}} = N/V$ is constant, CCN_{ret2} = the N/V is a function of r_{eff}, and CCN_{MAS} is the standard output from MAS algorithm.

Table 8. In situ Measurement of Several Parameters for Two Profiles (1600–1616 and 1902–1908 h UTC) During Flight 1733

Parameters	Measured Value		Remark
	1600–1616 h UTC	1902–1908 h UTC	
$V_{\text{in situ}}$, cm^3/m^2	0.0341 (0.002)	0.0294 (0.0015)	Integrated Dry Volume from the PCASP instrument
RH, %	77.47 (2.37)	76.97 (2.37)	Integrated Ambient RH
γ	0.71	0.71	Hygroscopicity measurement from *Kotchenruther et al.* [1999] for this flight
FRH(RH, γ)	2.16 (0.28)	2.11 (0.26)	Integrated hygroscopic factor (correction from ambient to PCASP RH)
$N_{\text{tot}} \times 10^8$, part/$cm^2$	5.1792 (0.0043) All bins 5.1730 (0.0042) Bins 1–8	4.3732 (0.0031) All bins 4.3695 (0.0031) Bins 1–8	Total number of particles in the column (PCASP)
Mass scattering efficiency, m^2/g	2.1	2.1	Derived by *Hegg et al.* [1997] in this flight.
ω_o	0.95	0.95	Derived by *Hegg et al.* [1997]
Ratio N/V, $1/\mu m^3$	218 (1)	218 (1)	Derived by *Hegg and Kaufman* [1999]
Dry r_{eff}, μm	0.1391 0.1382	0.1348 0.1355	= mean($V_{\text{tot}}(z)/S_{\text{tot}}(z)$) = $\int r_{\text{eff}}(z)dz/\Delta z$
Dry η	0.8899 0.8596	0.9178 0.8967	= mean($V_{\text{acc}}/V_{\text{tot}}$) = mean($\sigma_{sp}$(accu)/$\sigma_{sp}$(total))
Ambient Temperature	T(z = 0.03 km) = 22.2 T(z = 1.84 km) = 14.7	T(z = 0.07 km) = 22.2 T(z = 1.26 km) = 17.1	Measured at top and bottom of the profile

1903:22 and 1905:22 h UTC (columns 4 and 5) particle concentration goes up (~5800 #/cm^3) and scattering coefficient rises, too, in a layer of 300 meters. However, no noticeable gradient is seen in the optical depth in this range, suggesting compensating changes in aerosol vertical structure outside the C131 flight path.

[74] The integrated measurements from two of the three C131 profiles are shown in Table 8. The profile taken at 1600 h UTC is shown because it was done in the same area and gives an idea of the changes of columnar averages over time. In Figure 9, two rows of panels display the respective scattering coefficient, ambient T, RH and aerosol concentrations. Both profiles show large aerosol concentrations divided into two layers (0–0.35 km and 0.35–0.9 km) in the column with humidities above 70% (up to 1.5 km). Note that the levels of scattering are similar in both layers and in both profiles. In particular, in the top layer of the first profile the ambient humidity is above 80%. However, there is no large hygroscopic effect, as can be seen in the left panels of Figure 9 which look similar in magnitude for the dry and quasi-ambient σ_{sp}'s in the two profiles. As indicated by the difference in aerosol concentrations in the two profiles, it appears that the higher σ_{sp} expected (because of the higher RH) is compensated by the decrease in concentration in the first profile with respect to the second.

[75] In the case of the profile taken closest in time with the ER-2 pass (1902–1908 h UTC), it is difficult to compare the profile data with specific pixels since the profile is representative of several pixels in the MAS picture. However, it is clear that the retrieved volumes (new and Fraser methods, ~0.029 and ~0.023 cm^3/m^2 respectively) are close to the true value (0.0294 cm^3/m^2) in the pixels corresponding to the beginning of the profile (1902:00–1903:52 h UTC), with the new method closer to the true value than the Fraser method. At the end of the profile, the new method still approximates the true value better than the Fraser method.

[76] The in situ η is significantly higher than the MAS η for most of the profile. The ratio between in situ and retrieved r_{eff} varies, depending on the selected pixel, between 0.8 and 1.5 μm. Since the MAS r_{eff} is in ambient conditions, it was corrected by a factor of 1.15 to dry conditions prior to obtain the parameterized mse for the pixel. The same correction was applied to r_{eff} before utilization in equation (13). Similarly to the case of flight 1728, the CCN concentrations derived with the constant N/V ratio and the variable N/V method fared better than the MAS retrieval, in this case much more decisively.

5. Application on MODIS Pictures

[77] Terra was launched on 19 December 1999 and some of the operational Level 2 Atmospheric products (i.e., radiances that have been processed by the different atmospheric algorithms) have become available to the scientific community for general evaluation and testing. The aerosol (labeled MOD04L2) and column water vapor (MOD05L2) products became available starting on 22 August 2000 and temperature and moisture profiles (MOD07L2) became available on 20 October 2000. The retrieval algorithms for all these products are still considered to be in the developmental stage and the products are considered as beta versions that may be reprocessed a posteriori. We take advantage of some of this data to further explore the viability of our retrievals, specifically we show retrievals of aerosol dry mass and CCN concentration for an episode of Saharan dust advecting to the Atlantic ocean.

[78] At the time of this write-up, validation tests of the aerosol products are being conducted [*Chu et al.*, 2002; *Ichoku et al.*, 2002; *Remer et al.*, 2002]. For example, it has been established that the aerosol over land products are accurate to within their calculated uncertainties ($\pm$ 0.05 $\pm$ 0.20*τ [*Chu et al.*, 2002]), except in situations with possible cloud contamination over surfaces with subpixel surface water such as coastal areas and marshes, and over

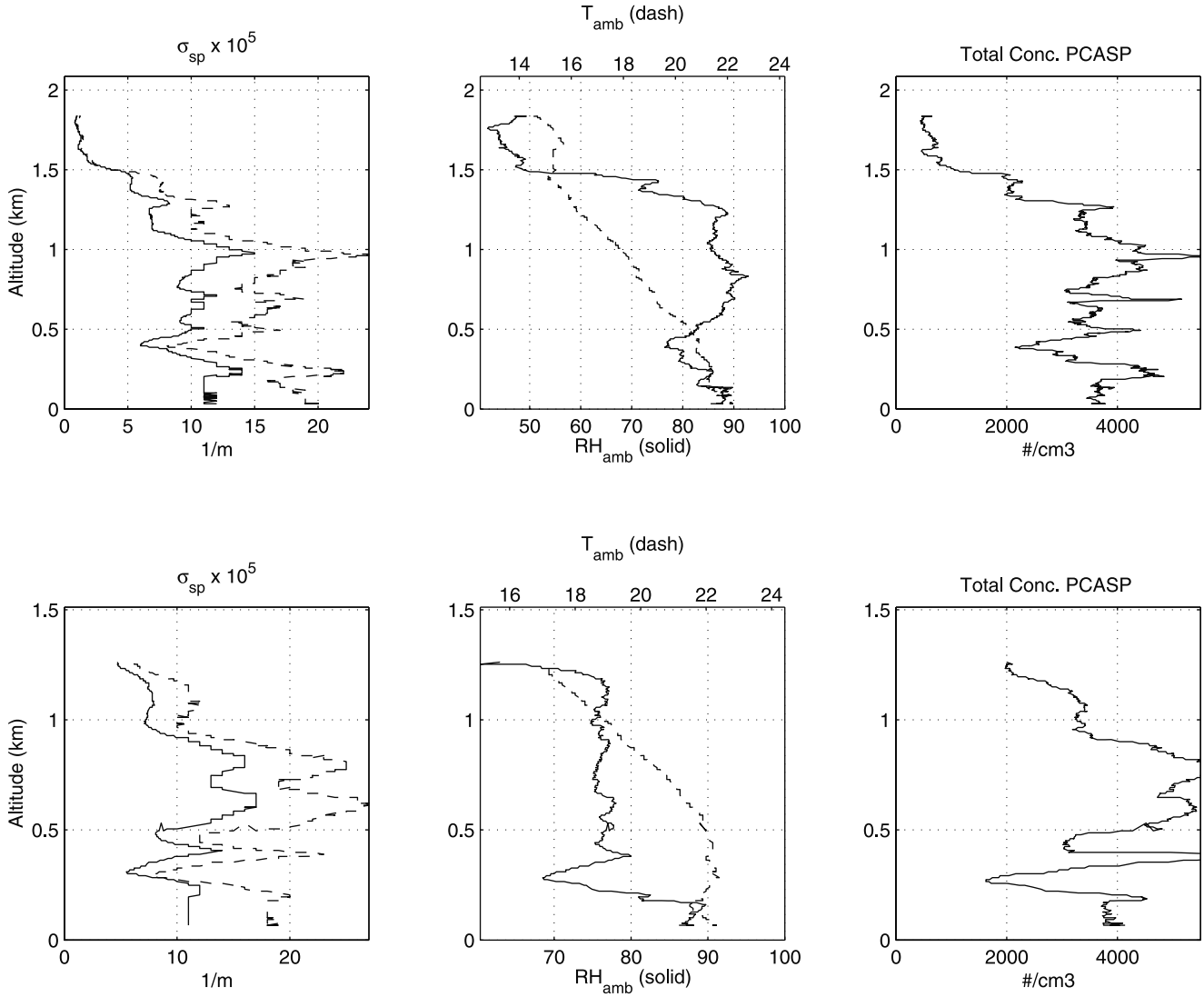

Figure 9. Profile of dry and almost-ambient σ_{sp} (left panel, solid and dash lines respectively), ambient T and RH (center) and total aerosol concentration in flight 1733 used for comparison with MAS data. Top row is the profile taken at 1660–1616 h UTC and bottom row is the profile taken at 1902–1908 h UTC.

surfaces with subpixel snow or ice cover. In addition, the aerosol over ocean optical thickness products are accurate to within their calculated uncertainties ($\pm$ 0.03 $\pm$ 0.05*τ [*Remer et al.*, 2002]). Since the deployment of Terra, a number of experiments have been conducted (ACE-Asia, PRIDE, CLAMS) with coordinated flights between in situ platforms and Terra passes.

[79] On 12 February 2001 a large low pressure center developed over the central region of the North Atlantic ocean, coupled along with a high pressure centers located over the Mediterranean sea and a second one located over the Azores Is. A resultant large region of constant easterly winds extending from approximately 28° to 13°N (Figure 10, bottom panel) transported a large dust cloud from the Saharan desert over the Atlantic. The METEOSAT visible picture indicates the extension of the plume and it shows that it is transported northward by the Azores high. The dust is remarkably bright, indicating the presence of heavy aerosol loading (Figure 10, top panel). The dry air coming off the Saharan desert results in little cloud formation downwind, which makes it a good case for satellite analysis. Additionally, the high-pressure center located over the Mediterranean Sea possibly transported European pollution and dry air from the north coast of Africa toward the Iberian Peninsula.

[80] Terra pictures (1135 and 1140 h UTC) corresponding aerosol products are shown in Figure 11. Note that the color-coding is in logarithmic scale to facilitate the display of the gradients in the low aerosol loading near Spain. Optical depths higher than 1.5 are all color coded with the same color black. The dust cloud appears to be well localized west of 17° longitude with a transition region over the Canary Islands. The low optical depths in the Spain–Canary Is. corridor is typical of small aerosol loadings and frequently found in marine environments [*Durkee et al.*, 2000]. Notice the east–west streak of high OD's in the Gibraltar Strait. Given the synoptic situation outlined, the higher OD can be caused by pollution advected from

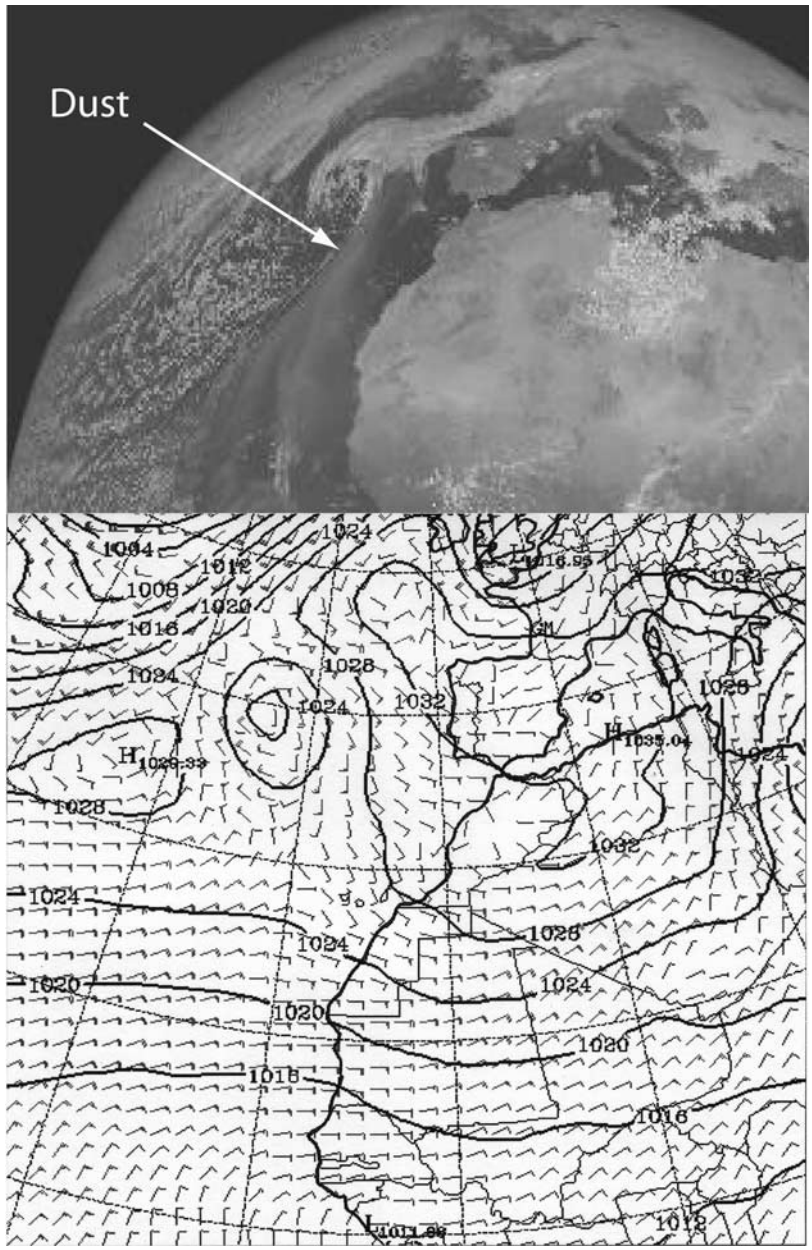

Figure 10. METEOSAT picture (visible) taken on 12 February 2001 at 1135 h UTC (top panel). Bottom panel is the NCEP model forecast for the surface winds and pressure for the same day.

Europe, sea salt or continental dust from North Africa. It is at this point that the additional parameters retrieved by the MODIS aerosol algorithm can help to distinguish the aerosol type. Figures 11b and 11c display the retrieved effective radius and η for the same scene. As expected, the suspected dust r_{eff}'s are high (i.e., above 0.4 μm), with increasing values toward the areas of higher burden, along with a small η (0.3–0.4) consistent with an aerosol with large coarse mode contribution. Outside the dust cloud, the r_{eff} ranges from 0.12 to 0.4 μm and the corresponding η ranges 0.85–0.99. The east–west streak in the Gibraltar strait has values of $\eta \sim 0.3–0.4$ and $r_{eff} \sim 0.5–0.7$ μm. These values are more consistent with aerosol size distributions that have an important contribution of coarse mode particles, i.e., wind generated sea salt aerosols or continental dust rather than advected pollution.

[81] Figure 11d displays the hygroscopic correction factor ($FRH = ((1-RH)/(1-RH_o))^{-\gamma}$ for reference $RH_o = 30\%$ and $\gamma = 0.7$) and it was derived from the mean RH for the bottom four layers in the BL (approximately 2.0 km). The factor FRH is computed only where $\tau < 0.4$ and it is set to 1 in pixels with higher OD's under the assumption that these higher OD's correspond to dust and dust plumes tend to advect in the free dry troposphere as in the cases observed during ACE-2 [*Collins et al.*, 2000; *Gassó et al.*, 2000]. The correction for humidity would thus be minimal.

[82] Figure 12 shows the retrieval of ambient (i.e., no correction for humidity applied) mass burden from the MODIS operational product (panel A), the new method developed here (panel B) and the Fraser method (panel C). Since the focus of this section is to illustrate the qualitative features and differences of the two methods for dry mass

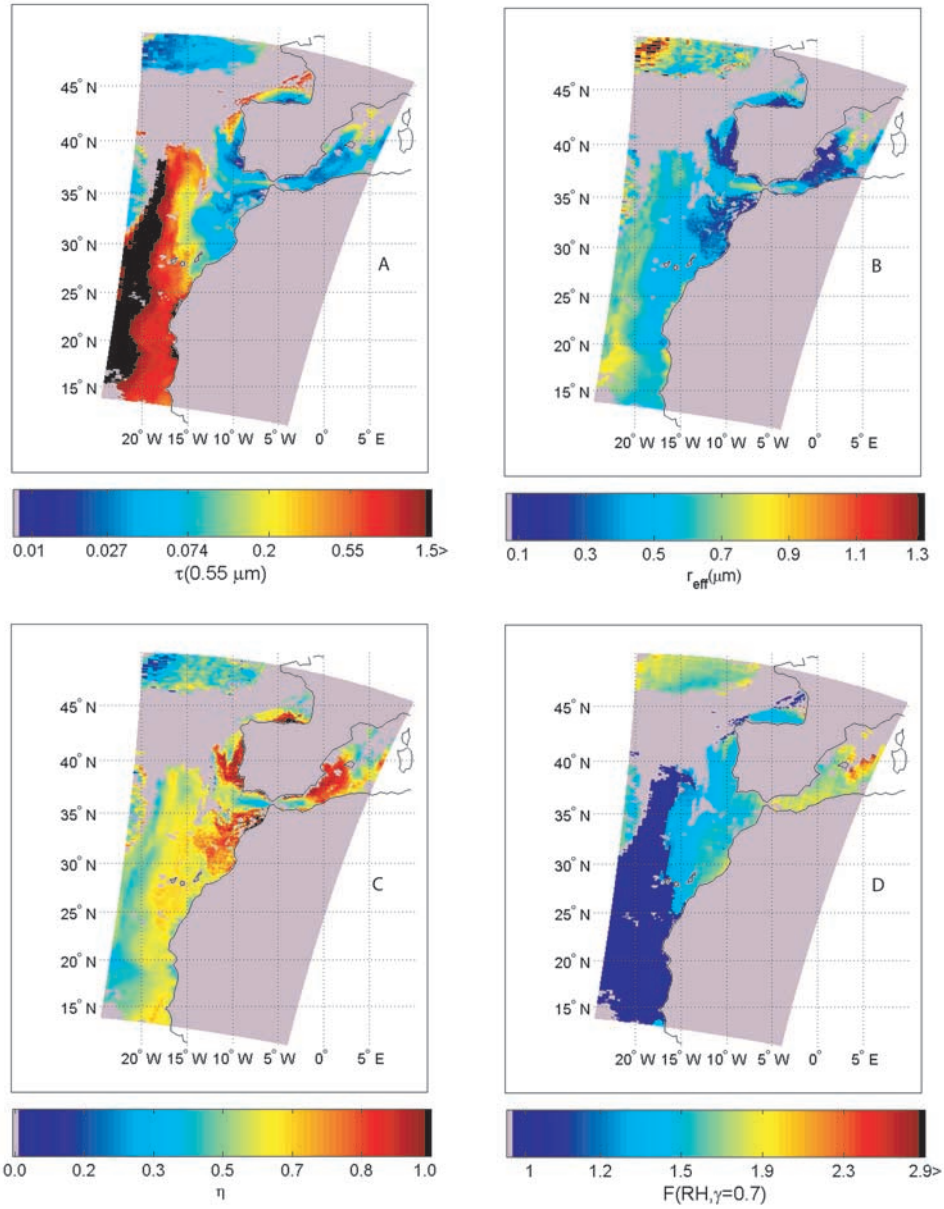

Figure 11. MODIS operational retrieval of aerosol and moisture parameters. Aerosol optical depth (0.550 μm, average, panel A), Effective radius in um (Panel B), Contribution of the small mode to total radiance (Panel C) and Humidity correction factor (Panel D) computed from the mean RH in bottom 4 layers and for a constant $\gamma = 0.7$ (reference $RH_o = 30\%$). $F(RH, \gamma) = 1$ in dust (i.e., $\tau > 0.4$).

retrieved that arise from the use of RH correction and a parameterized mse, all the retrievals assumed a single scattering albedo (ω_o) of 1.0 and an aerosol density of 1.7 g/cm^3. The MODIS aerosol algorithm computes the ambient total burden (or total columnar mass, mass/area) as a function of the size distribution parameters retrieved, r_{eff} and η but assumes a constant density of 1 g/m^3 (Note that we have corrected the MODIS algorithm for a missing $4\pi/3$ factor).

[83] The center panel of Figure 12 displays the ambient columnar mass derived with a variable mass scattering efficiency (using equation (12)). In panel C, the columnar ambient mass is computed with a constant mass scattering efficiency (Fraser method). The latter considered two mass scattering efficiencies depending on whether the pixel was thought to contain dust or not. Pixels with high OD ($\tau > 0.4$) were considered as dust and the respective dry mass scattering efficiency was set to 0.2 m^2/g, whereas in pixels with low OD ($\tau < 0.4$), the dry mass scattering efficiency was set to 2.0 m^2/g. In the case of variable mse, the humidity effect is considered since mse is computed as a function of the ambient r_{eff} and η. Note the sharp contrast of mass retrieved between dust and nondust pixels for the Fraser method (from red to yellow in the right panel), a consequence of assuming a constant mse in the scene.

[84] Comparison of the three panels indicates that the MODIS operational retrieval is about two orders of magnitude smaller relative on the other hand, the Fraser method and the new method are within the same magnitude range.

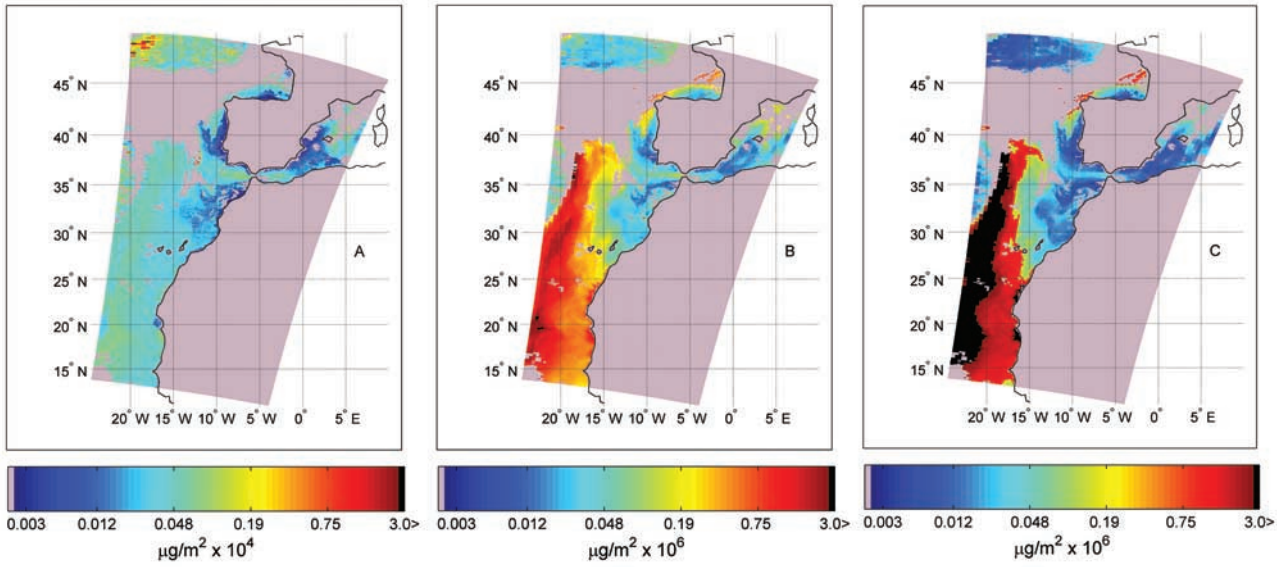

Figure 12. Ambient Columnar aerosol mass derived by three methods. Standard output from the MODIS operational algorithm (panel A) which assumes $\rho = 1.0$ g/cm^3 and it includes a factor $4\pi/3$ missing in the algorithm. Derivation with a variable mse (panel B, assumed $\rho = 1.7$ g/cm^3) and with a constant mse (mse = 0.4 m^2/g for $\tau > 0.4$ and mse = 2.0 m^2/g for $\tau < 0.4$, assumed $\rho = 1.7$ g/cm^3, panel C). Note the different scaling factor in Panel A ($\times 10^4$) with respect to B and C ($\times 10^6$). The color scale is logarithmic.

Unfortunately no in situ data are available for comparison with data from this picture. However, with a few assumptions it is possible to compare literature values. For example, assuming that all the aerosol mass is concentrated in a 1 km layer, the dust concentration at 30N, 16W (right west of the Canary Is.) will be 0.5, 500–800 and above 1000–3000 μg/m^3 for the three panels respectively from left to right. Among the three retrievals, the variable mse method seems most reasonable according to literature values for dust mass concentrations [*Li-Jones et al.*, 1998; *Campanelli et al.*, 2001].

[85] Figure 13 is an example of retrieval of CCN concentration computed from the retrieved dry mass and from the standard output of the MODIS operational retrieval shown in Figure 12. Panel B was computed by using a constant N/V ratio (=200 1/μm^3 [*Hegg and Kaufman*, 1998]) and panel C uses a variable N/V ratio as defined by equation (13) (it is important to note that the utilization of the N/V ratios implies retrievals of CCN active at supersaturation ~0.1%). Since retrievals of water vapor profiles are only available in nondust region, the figure shows retrievals only in the clean region.

[86] In order to compare with real concentrations, it is useful to assume, once again, that all particles are concentrated in 1.0 km layer. Thus, a columnar concentration of 2×10^8 CCN/cm^2 would be equivalent to a concentration of

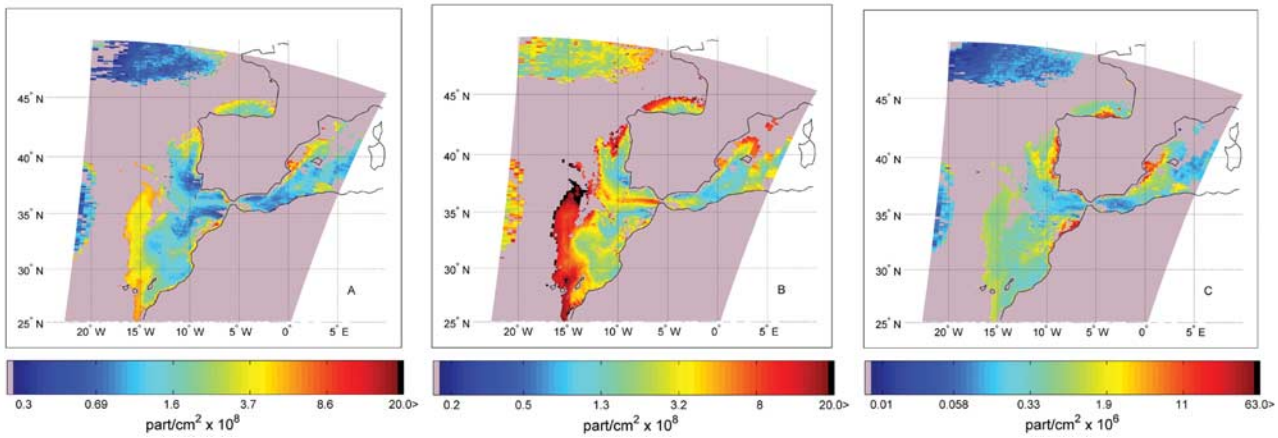

Figure 13. Retrievals of columnar CCN concentration (number of particles/area) based on the volume retrievals of Figure 12. Panel A is the standard operational product from the MODIS algorithm. Panel B using new method with a constant N/V ratio (=200 1/μm^3) and Panel C using variable N/V ratio (f(r_{eff}) as in equation (13)).Note the change in scaling factor in Panel C. The color scale is logarithmic.

2000 CCN/cm^3, typical of polluted plumes. In inter-comparing the nondust region of the 3 panels, it is clear that the retrievals using a variable N/V ratio (Panel C) underestimates (by a factor of 100) the number concentration commonly found in the marine environment. For example, it derives concentrations of the order of 1–10 CCN/cm^3 in the Tenerife-Spain corridor. Panels A and B display values that are slightly more in agreement with the expected ranges in the North Atlantic i.e., concentrations ranging 10–1000 CCN/cm^3. However, the values in the Canary Is-Spain corridor for both panels A and B seem to be in the 500–2000 CCN/cm^3 range. During ACE-2, *Chuang et al.* [2000] found CCN concentrations at 0.1% supersaturation in precisely this area averaged ~100 CCN/cm^3 and never exceeded 550 CCN/cm^3 even under polluted conditions. Hence, it is not entirely clear which retrieval algorithm is more accurate. Also, note that the MODIS operational retrievals are smaller in magnitude than the new method and that it is not as sensitive as details as the new method is. For example, note that Panel B shows gradients in the Gibraltar strait that are not observed in Panel A.

6. Summary and Concluding Remarks

[87] An improvement in an existing method (the Fraser method) for the retrieval of aerosol mass was introduced. Conceptually, the Fraser method relies on a measurement of aerosol optical depth and a number of assumptions on ambient humidity and aerosol composition to derive the columnar dry mass. The Fraser method has the drawback that it cannot be implemented in an automatic retrieval since it requires information on the aerosol composition that can only be incorporated during the postprocessing of the data by the data user. The new method is geared toward automatic retrieval. Although the new method uses the same basic concept (i.e., proportionality between optical depth and columnar mass), it makes use of some additional information available from newer platforms that help to constrain some of the parameters assumed in the Fraser method. For example, the new method makes use of the estimation of ambient humidity retrieved by the infrared channel in the MODIS detector. Hence the columnar dry mass is derived in each pixel as opposed to the Fraser method that assumes the same humidity correction for the whole picture. In addition we used the parameters r_{eff} and η (standard outputs of the MODIS aerosol algorithm in each pixel) to derive a mass scattering efficiency consistent with those parameters. This is another improvement with respect to the Fraser method, which assumed a constant mse for the whole picture. These are the two major improvements in the new method.

[88] We provided a detailed comparison of the two methods by analyzing columnar dry aerosol volumes derived from in situ instrumentation with aerosol volumes derived from sunphotometer optical depths. To the extent of our bibliographical research, this is the first time that the method has been validated with in situ measurements from aircraft. With measurements drawn from the ACE-2 data set, we compared retrievals of columnar volumes in Saharan dust in conditions of low ambient humidity. We showed that the Fraser method achieves reasonable retrievals (r^2 = 0.86) indicating that if the aerosol type is known, the retrieval can be implemented at least in dry conditions. The new method proposed here fared better (r^2 = 0.99), indicating that the customization of the mse to the pixel under observation improves the retrieval. However, the data available for the validation of dust retrievals was limited (eight profiles from two flights, all with similar r_{eff} and η). Thus, the method requires further validation with a more comprehensive data set.

[89] The retrieval of aerosol dry volume in conditions of high humidity was studied in section 3.2. In this case, a correction factor that depends explicitly on an estimation of the mean relative humidity in the layer was utilized to bring the ambient optical depth to dry conditions. The TARFOX data set, containing several profiles with aerosol layers with high ambient humidity, was utilized to validate the retrievals. In this case, the retrieval of dry volumes was less precise and the new method did not show a clear improvement with respect to the Fraser method (Table 3). A number of reasons for this were discussed. Among these, the most notable are the reliability of the in situ measurements to reconstruct the optical properties of aerosol and the assumption of a constant humidity correction to account for the hygroscopic effects.

[90] In section 4, we employed an algorithm on actual remote sensing data. Specifically, we showed a comparison of volumes derived from two flights of the MODIS Airborne Simulator made during TARFOX in coordination with profiles taken by the C131 aircraft (C131 flights 1728 and 1733). Additionally, we utilized the *Hegg and Kaufman* [1998] parameterization to derive the columnar number CCN concentrations from the retrieved volumes and compared these with the same parameters retrieved by MAS. For both the dry mass and CCN concentration, the new algorithm returned values closer to in situ measurements than the existing techniques.

[91] The results achieved by using the new method for mass volume and number retrieval are encouraging. However, they clearly require further validation. For example, although the improvements proposed here seem to work better than the Fraser method, the differences between the two methods when comparing with the true values are not very large. The variability of some the parameters assumed (ρ, ω_o, γ), along with the uncertainty in r_{eff} and η could shift the retrieved values away from the true one. Additionally, when using optical particle counters in computing in situ columnar volumes, the calibration of the instrument is very important in establishing the true values of aerosol volume.

[92] The assumption of constant RH and mse in the column needs further study. We showed examples where these assumptions work well (when there are thin layers of ambient RH and aerosol concentrations in the column, top panels in Figure 9). However, we showed that when the humidity is high (above 90%) and in thick layers, the retrievals for either of the two methods are poor. Thus, it is necessary to explore further the conditions where the constant RH and mse assumptions are valid and establish if there are any flags (such as vertical profiles of humidity) that can be used to determine the level of confidence of the retrieval.

[93] Finally, we applied both methods to an actual MODIS picture and retrieved aerosol mass burden and columnar CCN concentrations and compared them against the same

parameters derived by the MODIS operational retrieval. Although we do not have simultaneous in situ measurements to validate the retrievals, we showed that the proposed methods yield more credible values than the MODIS retrievals of columnar mass.

[94] The analysis demonstrates how difficult validation of aerosol airborne retrievals can be. There are not only limitations due to the coordination of platforms, incomplete information and instrumentation inefficiencies but also some important limitations which go beyond the technological or logistic shortcomings. For example, until recently validation of satellite retrievals was limited to comparisons of optical depths. The validation of columnar retrievals such as r_{eff} or aerosol mass pose new challenges to the scientific community. The work shown here was an attempt to address this issue, at least in a preliminary sense.

[95] **Acknowledgments.** This project was supported by NASA Earth System Science Fellowship (NGT-30121), grant NAG-8684 and ONR grant number N00014-97-1-0132. The authors wish to thank the MODIS aerosol group in Greenbelt, MD for facilitating access to the algorithms and data.

References

Ackerman, S. A., K. I. Strabala, W. P. Menzel, R. A. Frey, C. C. Moeller, and L. E. Gumley, Discriminating clear sky from clouds with MODIS, *J. Geophys. Res.*, *103*(D24), 32,141–32,157, 1998.

Albrecht, B. A., Aerosols, cloud microphysics, and fractional cloudiness, *Science*, *245*(4923), 1227–1230, 1989.

Andreae, T. W., M. O. Andreae, C. Ichoku, W. Maenhaut, A. Cafmeyer, J. Karnieli, and L. Orlovsky, Light scattering by dust and anthropogenic aerosol at a remote site in the Negev desert, Israel, *J. Geophys. Res.*, *107*(D1), doi:10.1029/2001JD900252, 2002.

Boucher, O., and U. Lohmann, The sulfate-CCN-cloud albedo effect: A sensitivity study with two general circulation models, *Tellus, Ser. B*, *47*(3), 281–300, 1995.

Brenguier, J. L., et al., An overview of the ACE-2 CLOUDYCOLUMN closure experiment, *Tellus, Ser. B*, *52*(2), 815–827, 2000.

Campanelli, M., W. Junkermann, B. Olivieri, and G. Tonna, Physical features of the atmospheric aerosol determined with an aureolemeter and a FSSP probe in the Mediterranean Lampedusa island, *Atmos. Environ.*, *35*(21), 3607–3618, 2001.

Carlson, T. N., and R. S. Caverly, Radiative characteristics of Saharan dust at solar wavelengths, *J. Geophys. Res.*, *82*(21), 3141–3152, 1977.

Carrico, et al., Aerosol optical properties at Sagres, Portugal during ACE-2, *Tellus, Ser. B*, *52*(2), 694–715, 2000.

Chin, M., P. Ginoux, S. Kinne, O. Torres, B. N. Holben, B. N. Duncan, R. V. Martin, J. A. Logan, A. Higurashi, and T. Nakajima, Tropospheric aerosol optical thickness from the GOCART model and comparisons with satellite and sun photometer measurements, *J. Atmos. Sci.*, *59*(3), 461–483, 2002.

Chu, A., Y. J. Kaufman, C. Ichoku, L. A. Remer, D. Tanré, and B. N. Holben, Validation of MODIS aerosol optical depth over land, *Geophys. Res. Lett.*, *29*(12), doi:10.1029/2001GL013205, 2002.

Chu, D. A., Y. J. Kaufman, L. A. Remer, and B. N. Holben, Remote sensing of smoke from MODIS airborne simulator during the SCAR-B experiment, *J. Geophys. Res.*, *103*(D24), 31,979–31,988, 1998.

Chuang, P. Y., D. R. Collins, H. Pawlowska, J. R. Snider, H. H. Jonsson, J. L. Brenguier, R. C. Flagan, and J. H. Seinfeld, CCN measurements during ACE-2 and their relationship to cloud microphysical properties, *Tellus, Ser. B*, *52*(2), 843–867, 2000.

Clarke, A. D., J. N. Porter, F. P. J. Valero, and P. Pilewskie, Vertical profiles, aerosol microphysics, and optical closure during the Atlantic Stratocumulus Transition Experiment: Measured and modeled column optical properties, *J. Geophys. Res.*, *101*(D2), 4443–4454, 1996.

Clarke, A. D., W. G. Collins, P. J. Rasch, V. N. Kapustin, K. Moore, S. Howell, and H. E. Fuelberg, Dust and pollution transport on global scales: Aerosol measurements and model predictions, *J. Geophys. Res.*, *106*(D23), 32,555–32,570, 2001.

Collins, D. R., et al., In situ aerosol-size distributions and clear-column radiative closure during ACE-2, *Tellus, Ser. B*, *52*(2), 498–525, 2000.

Dulac, F., D. Tanré, G. Bergametti, P. Buat-Menard, M. Desbois, and D. Sutton, Assessment of the African airborne dust mass over the western Mediterranean Sea using METEOSAT data, *J. Geophys. Res.*, *97*(D2), 2489–2506, 1992.

Durkee, P. A., F. Pfeil, E. Frost, and R. Shema, Global analysis of aerosol particle characteristics, *Atmos. Environ.*, *Part A*, *25*(11), 2457–2471, 1991.

Durkee, P. A., et al., Regional aerosol optical depth characteristics from satellite observations: ACE-1, TARFOX and ACE-2 results, *Tellus, Ser. B*, *52*(2), 484–497, 2000.

Ferrare, R. A., R. S. Fraser, and Y. J. Kaufman, Satellite measurements of large scale air pollution: Measurements of forest fire smoke, *J. Geophys. Res.*, *95*(D7), 9911–9925, 1990.

Fitzgerald, J. W., Dependence of supersaturation spectrum Of CCN on aerosol size distribution and composition, *J. Atmos. Sci.*, *30*(4), 628–634, 1973.

Fouquart, Y., B. Bonnel, G. Brogniez, J. C. Buriez, L. Smith, J. J. Morcrette, and A. Cerf, Observations of Saharan aerosols—Results of Eclats Field Experiment, 2, Broad-band radiative characteristics of the aerosols and vertical radiative flux divergence, *J. Appl. Meteorol.*, *26*(1), 38–52, 1987.

Fraser, R. S., Satellite measurement of mass of Sahara dust in the atmosphere, *Appl. Opt.*, *15*(10), 2471–2479, 1976.

Fraser, R. S., Y. J. Kaufman, and R. L. Mahoney, Satellite measurements of aerosol mass and transport, *Atmos. Environ.*, *18*(12), 2577–2584, 1984.

Gassó, S., and D. A. Hegg, Comparison of columnar aerosol optical properties measured by the MODIS airborne simulator with in situ measurements: A case study, *Remote Sens. Environ.*, *66*(2), 138–152, 1997.

Gassó, S., et al., Influence of humidity on the aerosol scattering coefficient and its effect on the upwelling radiance during ACE-2, *Tellus, Ser. B*, *52*(2), 546–567, 2000.

Griggs, M., Measurements of atmospheric aerosol optical thickness over water using ERTS-1 data, *J. Air Pollut. Control Assoc.*, *25*(6), 622–626, 1975.

Hänel, G., The properties of atmospheric aerosols as functions of the relative humidity at thermodynamic equilibrium with surrounding air, *Adv. Geophys.*, *19*, 73–188, 1976.

Hartley, W. S., Airborne study of aerosol optical properties and direct aerosol radiative forcing off the east coast of the United States, M.S. thesis, Univ. of Wash., Seattle, 2000.

Hartley, W. S., P. V. Hobbs, J. L. Ross, P. B. Russell, and J. M. Livingston, Properties of aerosols aloft relevant to direct radiative forcing off the mid-Atlantic coast of the United States, *J. Geophys. Res*, *105*(D8), 9859–9885, 2000.

Haywood, J. M., and V. Ramaswamy, Global sensitivity studies of the direct radiative forcing due to anthropogenic sulfate and black carbon aerosols, *J. Geophys. Res.*, *103*(D6), 6043–6058, 1998.

Haywood, J. M., D. L. Roberts, A. Slingo, J. M. Edwards, and K. P. Shine, General circulation model calculations of the direct radiative forcing by anthropogenic sulfate and fossil-fuel soot aerosol, *J. Clim.*, *10*(7), 1562–1577, 1997.

Hegg, D. A., and H. H. Jonsson, Aerosol number-to-volume relationship and relative humidity in the eastern Atlantic, *J. Geophys. Res.*, *105*(D2), 987–995, 2000.

Hegg, D. A., and Y. J. Kaufman, Measurements of the relationship between submicron aerosol number and volume concentration, *J. Geophys. Res.*, *103*(D5), 5671–5678, 1998.

Hegg, D. A., D. S. Covert, M. J. Rood, and P. V. Hobbs, Measurements of aerosol optical properties in marine air, *J. Geophys. Res.*, *101*(D8), 12,893–12,904, 1996.

Hegg, D. A., J. Livingston, P. V. Hobbs, T. Novakov, and P. Russell, Chemical apportionment of aerosol column optical depth off the mid-Atlantic coast of the United States, *J. Geophys. Res.*, *102*(D21), 25,293–25,303, 1997.

Hitzenberger, R., and R. Rizzi, Telephotometer measurements and retrieved mass increase coefficients of the aerosol size distribution, *Nuovo Cimento Soc. Ital. Fis.*, *16C*(C2), 107–129, 1993.

Hobbs, P. V., An overview of the University of Washington airborne measurements and results from the Tropospheric Aerosol Radiative Forcing Observational Experiment (TARFOX), *J. Geophys. Res.*, *104*(D2), 2233–2238, 1999.

Holben, B. N., et al., An emerging ground-based aerosol climatology: Aerosol optical depth from AERONET, *J. Geophys. Res.*, *106*(D11), 12,067–12,097, 2001.

Hsu, S. A., and B. W. Blanchard, The relationship between total precipitable water and surface-level humidity over the sea surface: A further evaluation, *J. Geophys. Res.*, *94*(C10), 14,539–14,545, 1989.

Husar, R. B., J. M. Prospero, and L. L. Stowe, Characterization of tropospheric aerosols over the oceans with NOAA Advanced Very High Resolution Radiometer optical thickness operational product, *J. Geophys. Res.*, *102*(D14), 16,889–16,909, 1997.

Ichoku, C., A. Chu, S. Mattoo, Y. J. Kaufman, L. A. Remer, D. Tanré, I. Slutsker, and B. N. Holben, A spatio-temporal approach for global

validation and analysis of MODIS aerosol products, *Geophys. Res. Lett.*, *29*(12), doi:10.1029/2001GL013206, 2002.
Kasten, F., Visibility in the phase of pre-condensation, *Tellus*, *21*, 631–635, 1969.
Kaufman, Y. J., and R. S. Fraser, Light extinction by aerosols during summer air pollution, *J. Clim. Appl. Meteorol.*, *22*(10), 1694–1706, October 1983.
Kaufman, Y. J., and R. S. Fraser, Satellite measurements of large-scale air pollution: Methods, *J. Geophys. Res.*, *95*(D7), 9895–9909, 1990.
King, M. D., Y. J. Kaufman, W. P. Menzel, and D. Tanré, Remote sensing of cloud, aerosol, and water vapor properties from the moderate resolution imaging spectrometer (MODIS), *IEEE Trans. Geosci. Remote Sens.*, *30*(1), 2–27, 1992.
King, M. D., et al., Airborne scanning spectrometer for remote sensing of cloud, aerosol, water vapor, and surface properties, *J. Atmos. Oceanic Technol.*, *13*(4), 777–794, 1996.
Kotchenruther, R. A., P. V. Hobbs, and D. A. Hegg, Humidification factors for atmospheric aerosol off the mid-Atlantic coast of United States, *J. Geophys. Res.*, *104*(D2), 2239–2251, 1999.
Langner, J., and H. Rodhe, A global three-dimensional Model of the tropospheric sulfur cycle, *J. Atmos. Chem.*, *13*, 225–263, 1991.
Li-Jones, X., H. B. Maring, and J. M. Prospero, Effect of relative humidity on light scattering by mineral dust aerosol as measured in the marine boundary layer over the tropical Atlantic Ocean, *J. Geophys. Res*, *103*(D23), 31,113–31,121, 1998.
Liousse, C., F. Dulac, H. Cachier, and D. Tanré, Remote sensing of carbonaceous aerosol production by African savanna biomass burning, *J. Geophys. Res.*, *102*(D5), 5895–5911, 1997.
Malm, W. C., and D. E. Day, Optical properties of aerosols at Grand Canyon National Park, *Atmos. Environ.*, *34*(20), 3373–3391, 2000.
Maring, H., D. L. Savoie, M. A. Izaguirre, C. McCormick, R. Arimoto, J. M. Prospero, and C. Pilinis, Aerosol physical and optical properties and their relationship to aerosol composition in the free troposphere at Izana, Tenerife, Canary Islands during July 1995, *J. Geophys. Res.*, *105*(D11), 14,677–14,700, 16 June 2000.
Matsumoto, T., Airborne tracking sunphotometer, *J. Atmos. Oceanic Technol.*, *4*(2), 336–339, 1987.
Menzel, P., and L. Gumley, *MODIS: Atmospheric Profile Retrieval Algorithm Theoretical Basis Document, Version 4.0*, Univ. of Wis. Press, Madison, 1998.
Mishchenko, M. I., I. V. Geogdzhayev, B. Cairns, W. B. Rossow, and A. A. Lacis, Aerosol retrievals over the ocean by use of channels 1 and 2 AVHRR data: Sensitivity analysis and preliminary results, *Appl. Opt.*, *38*(36), 7325–7341, 1999.
Novakov, T., D. A. Hegg, and P. V. Hobbs, Airborne measurements of carbonaceous aerosols on the East Coast of the United States, *J. Geophys. Res.*, *102*(D25), 30,023–30,030, 1997.
Ogren, J. A., A systematic approach to in situ observations of aerosol properties, in *Aerosol Forcing of Climate*, edited by R. J. Charlson and J. Heintzenbeg, pp. 215–226, John Wiley, New York, 1995.
O'Neill, N. T., T. F. Eck, B. N. Holben, A. Smirnov, O. Dubovik, and A. Royer, Bimodal size distribution influences on the variation of Angstrom derivatives in spectral and optical depth space, *J. Geophys. Res.*, *106*(D9), 9787–9806, 2001.
Öström, E., and K. J. Noone, Vertical profiles of aerosol scattering and absorption measured in situ during the North Atlantic Aerosol Characterization Experiment (ACE-2), *Tellus, Ser. B*, *52*(2), 526–545, 2000.
Penner, J. E., R. E. Dickinson, and C. A. O'Neill, Effects of aerosol from biomass burning on the global radiation budget, *Science*, *256*(5062), 1432–1434, 1992.
Penner, J. E., C. C. Chuang, and K. Grant, Climate forcing by carbonaceous and sulfate aerosols, *Clim. Dyn.*, *14*(12), 839–851, 1998.
Penner, J. E., et al., A comparison of model- and satellite-derived aerosol optical depth and reflectivity, *J. Atmos. Sci.*, *59*(3), 441–460, 2002.
Quinn, P. K., D. J. Coffman, V. N. Kapustin, T. S. Bates, and D. S. Covert, Aerosol optical properties in the marine boundary layer during the First Aerosol Characterization Experiment (ACE 1) and the underlying chemical and physical aerosol properties, *J. Geophys. Res.*, *103*(D13), 16,547–16,563, 1998.
Raes, F., T. Bates, F. McGovern, and M. Van Liedekerke, The 2nd Aerosol Characterization Experiment (ACE-2): General overview and main results, *Tellus, Ser. B*, *52*(2), 111–125, 2000.
Ramanathan, V. P., J. Crutzen, J. T. Kiehl, and D. Rosenfeld, Aerosols, climate, and the hydrological cycle, *Science*, *294*, 2119–2124, 2001a.
Ramanathan, V., et al., Indian Ocean Experiment: An integrated analysis of the climate forcing and effects of the great Indo-Asian haze, *J. Geophys. Res.*, *106*(D22), 28,371–28,398, 2001b.
Redemann, J., et al., Retrieving the vertical structure of the effective aerosol complex index of refraction from a combination of aerosol in situ and remote sensing measurements during TARFOX, *J. Geophys. Res.*, *105*(D8), 9949–9970, 2000.
Reid, J. S., P. V. Hobbs, R. J. Ferek, D. R. Blake, and J. V. Martins, et al., Physical, chemical, and optical properties of regional hazes dominated by smoke in Brazil, *J. Geophys Res.*, *103*(D24), 32,059–32,080, 1998.
Reid, J. S., T. F. Eck, S. A. Christopher, P. V. Hobbs, and B. N. Holben, Use of the Angstrom exponent to estimate the variability of optical and physical properties of aging smoke particles in Brazil, *J. Geophys. Res*, *104*(D22), 27,473–27,489, 1999.
Remer, L. A., S. Gassó, D. A. Hegg, Y. J. Kaufman, and B. N. Holben, Urban/industrial aerosol: Ground-based Sun/sky radiometer and airborne in situ measurements, *J. Geophys. Res.*, *102*(D14), 16,849–16,859, 1997.
Remer, L. A., et al., Validation of MODIS aerosol retrieval over ocean, *Geophys. Res. Lett.*, *29*(12), doi:10.1029/2001GL013204, 2002.
Richards, L. W., S. H. Alcorn, C. McDade, T. Couture, D. Lowenthal, J. C. Chow, and J. G. Watson, Optical properties of the San Joaquin Valley aerosol collected during the 1995 integrated monitoring study, *Atmos. Environ.*, *33*(29), 4787–4795, 1999.
Rosenfeld, D., Y. Rudich, and R. Lahav, Desert dust suppressing precipitation: A possible desertification feedback loop, *Proc. Natl. Acad. Sci. U. S. A.*, *98*(11), 5975–5980, 2001.
Russell, P. B., and J. Heintzenberg, An overview of the ACE-2 clear sky column closure experiment (CLEARCOLUMN), *Tellus, Ser. B*, *52*(2), 463–483, 2000.
Russell, P. B., et al., Post-Pinatubo optical depth spectra vs. latitude and vortex structure: Airborne tracking sunphotometer measurements in AASE II, *Geophys. Res. Lett.*, *20*(22), 2571–2574, 1993.
Russell, P. B., P. V. Hobbs, and L. L. Stowe, Aerosol properties and radiative effects in the United States East Coast haze plume: An overview of the Tropospheric Aerosol Radiative Forcing observational Experiment (TARFOX), *J. Geophys. Res.*, *104*(D2), 2213–2222, 1999.
Schmeling, M., et al., Aerosol particle chemical characteristics measured from aircraft in the lower troposphere during ACE-2, *Tellus, Ser. B*, *52*(2), 185–200, 2000.
Schmid, B., et al., Clear sky closure studies of lower tropospheric aerosol and water vapor during ACE-2 using airborne sunphotometer, airborne in-situ, space-borne, and ground-based measurements, *Tellus, Ser. B*, *52*(2), 568–593, 2000.
Sheridan, P. J., and J. A. Ogren, Observations of the vertical and regional variability of aerosol optical properties over central and eastern North America, *J. Geophys. Res.*, *104*(D14), 16,793–16,805, 1999.
Strapp, W. L., W. R. Leaitch, and P. S. K. Liu, Hydrated and dried aerosol-size-distribution measurements from the particle measuring systems FSSP-300 probe and Deice PCASP-100X probe, *J. Atmos. Oceanic Technol.*, *9*, 548–555, 1992.
Tanré, D., Y. J. Kaufman, M. Herman, and S. Mattoo, Remote sensing of aerosol properties over oceans using the MODIS/EOS spectral radiances, *J. Geophys. Res.*, *102*(D14), 16,971–16,988, 1997.
Tanré, D., et al., Retrieval of aerosol optical thickness and size distribution over ocean from the MODIS airborne simulator during TARFOX, *J. Geophys. Res.*, *104*(D2), 2261–2278, 1999.

S. Gassó, NASA/GSFC, Code 913, Greenbelt, MD 20771, USA. (santiago@climate.gsfc.nasa.gov)
D. A. Hegg, Department of Atmospheric Science, University of Washington, Box 351640, Seattle, WA 98195, USA.